
The Right Answer, the Wrong Direction: Why Transformers Fail at Counting and How to Fix It

Gabriel Garcia
Independent Researcher
gpgabriel25@gmail.com

Abstract

Large language models often fail at simple counting tasks, even when the items to count are explicitly present in the prompt. We investigate whether this failure occurs because transformers do not represent counts internally, or because they cannot convert those representations into the correct output tokens.

Across three model families: Pythia, Qwen3, and Mistral, ranging from 0.4B to 14B parameters, we find strong evidence for the second explanation. Linear probes recover the correct count from intermediate layers with near-perfect accuracy ($R^2 > 0.99$), showing that the information is present. However, the internal directions that encode counts are nearly orthogonal to the output-head rows for digit tokens ($|\cos| \leq 0.032$). In other words, the model stores the count in a form that the digit logits do not naturally read out.

We localize this failure with two interventions. Updating only the digit rows of the output head (36,864 parameters) substantially improves constrained next-token digit prediction (60.7–100.0% across four tasks), but it does not fix unconstrained autoregressive generation (0% in our setting); we do *not* claim that digit-row repair fixes open-ended text. By contrast, a small LoRA intervention on attention Q/V weights (7.67M parameters) improves upstream routing and achieves $83.1\% \pm 7.2\%$ in true greedy autoregressive generation—the deployable fix we study. Logit-lens at layer 35 (entity counting, full-vocab rank of the correct digit) summarizes two *different* summaries of the same metric: **(i)** pooled median over 3 seeds drops from order- 10^4 to 1; **(ii)** seed 42 alone shows a trace $54,332 \rightarrow 838$ (the median can reach top-1 while an individual seed still sits far below). See §7. Additional norm, logit-lens, and cross-task analyses show that the bottleneck generalizes across character counting, addition, and list length, while remaining absent on MMLU and GSM8K and showing only limited partial transfer on DROP.

These results identify counting failure as a geometric readout bottleneck rather than a failure of internal representation: the model knows the count but the output pathway is geometrically misaligned with the tokens needed to express it.

1 Introduction

Core claims. This paper makes three nested claims:

- Geometric:** Count-encoding directions are orthogonal to `lm_head` digit rows ($|\cos| \leq 0.032$, indistinguishable from random). This is a structural property of the trained model, not a measurement artifact.
- Causal-diagnostic:** The 9-row repair localizes readout misalignment to digit rows under digit-restricted next-token evaluation (60.7–100.0% across tasks). Under unconstrained autoregressive generation the same weights yield 0%, so deployment-relevant failures include upstream routing beyond the output head alone.

- 3. Deployable:** LoRA Q/V rank-16 corrects upstream attention routing, achieving $83.1\% \pm 7.2\%$ greedy generation accuracy (5 seeds, multi-task; entity-only per-task: 97.0%, 96.5%, 94.5%). A locus ablation supports the routing-specificity interpretation (Q/V yields the strongest logit-lens alignment among single-projection variants).

Motivation. Large language models can perform multi-step reasoning, pass professional exams, and write functional code, but they count poorly. For controlled prompts of the form “*Count how many X there are in ...*,” the best models achieve $\leq 24\%$ accuracy without intervention, despite the task requiring no external knowledge beyond token-by-token reading. This is puzzling: counting errors cannot be explained as knowledge gaps, reasoning failures, or length-generalization breakdowns. Prior work has documented these failures without providing a principled explanation of *why* counting, specifically, breaks down when the answer is directly available in the input text.

We propose a geometric answer: the failure is a *readout bottleneck* at the output head: the model encodes counts accurately but the count-encoding direction is nearly orthogonal to the output head’s digit rows ($|\cos| \leq 0.032$). The diagnosis makes a falsifiable prediction: digit-row-only repair succeeds under constrained evaluation but fails in generation; upstream routing correction succeeds in both. Both hold, verified via logit-lens (*pooled median* rank $\sim 56k \rightarrow 1$ post-LoRA on entity counting; seed 42 on the same metric remains far below top-1; §7).

Mechanistic evidence for the LoRA Q/V route. We provide direct measurements at three points in the computation graph. At the count-encoding layer (layer 2), LoRA Q/V leaves the probe direction unchanged (mean $|\cos| = 0.0089 \rightarrow 0.0070$, 3 seeds); it does not rewrite early encoding. At the final transformer layer (layer 35), ridge-probe R^2 rises from 0.974 to 0.998 ($24\times$ residual amplification). Most directly, logit-lens analysis shows the correct digit’s median vocabulary rank drops from $\sim 55k$ to 1 post-LoRA (*pooled median* over 3 seeds; accuracy $9.3\% \rightarrow 71.8\%$; full-vocab rank at layer 35, entity counting): the output head directly reads the count from layer-35 hidden states. This mechanism generalizes across tasks: the same logit-lens improvement appears in character counting (rank $32,265 \rightarrow 1$) and addition (rank $21,186 \rightarrow 1$), with strength tracking task difficulty.

Scope. Our evidence is strongest for low-vocabulary aggregation tasks where internal representations are accurate but misaligned with the output head. Under one shared constrained next-token protocol on Qwen3-8B, probe-round reaches 96.8–100.0% and 9-row repair 60.7–100.0% across entity counting, character counting, addition, and list length (§6). The same bottleneck persists when the protocol changes: in instruct mode, first-token digit accuracy is only 22% despite $R^2 \geq 0.9996$, and the 9-row repair recovers 99.9% (3 seeds), confirming the misalignment is not a raw-completion artifact. Natural-language counting across 8 entity categories confirms generalization beyond synthetic templates (§6.3). MMLU and GSM8K confirm a clean null; DROP shows only limited partial transfer ($\sim +8$ pp; §7).

Contributions.

- 1. Geometric diagnosis and theoretical explanation:** We establish that count-encoding directions are orthogonal to `lm_head` digit rows ($|\cos| \leq 0.032$), and show empirically that this is a stable training equilibrium: gradients never align the count direction with digit rows when counting contexts represent a small fraction of digit-token occurrences in the training distribution (arithmetic fine-tuning does not reduce orthogonality; counting fine-tuning does). We further show that digit rows sit at the 12th–29th percentile of `lm_head` norms—structurally disadvantaged against 84% of the vocabulary—quantifying why open-vocabulary generation remains at 0% even after repair.
- 2. Causal localization via minimal diagnostic probe:** Fine-tuning only 9 output rows (36,864 params) raises constrained next-token accuracy from 10–24% to 60–100% (task-dependent), serving as a minimal causal probe that localizes the bottleneck to digit rows of the output head. This is a *diagnostic instrument*, not a deployable fix: the repair achieves 0% in autoregressive generation. The deployable fix—LoRA Q/V rank-16 (7.67M params) correcting attention routing—achieves $83.1\% \pm 7.2\%$ in true autoregressive generation (greedy decode; gap=0.000). At 14B scale, misalignment sharpens to $|\cos|=0.011$; mode-matched *row-only* repair reaches **58.2%** while soft DPS remains near baseline (10.8%). A separate **joint** pipeline—digit-row training *plus* hard DPS at decode on natural-language counting—

reaches $90.3\% \pm 1.5\%$ (Appendix Table 10), isolating the strong cross-scale gain in the readout pathway without claiming that 9-row weights alone hit 90%.

3. **Scope boundaries:** A Diagnostic Probe Steering auxiliary head (hard DPS: oracle digit-probe injected at each step) achieves 72.4% [69.6,75.4] in autoregressive generation—a diagnostic upper bound. Standard (soft) DPS under digit-restricted next-token evaluation returns to $\approx 13\%$, i.e., \approx the digit-restricted baseline, confirming the bottleneck is a routing failure, not a probe-direction failure. MMLU and GSM8K show no bottleneck effect; DROP shows only limited partial transfer (+8 pp).

What readers should take away. For bounded aggregation tasks, failures can arise not because the answer is absent from internal representations, but because the answer lives in a direction the output head does not read. This suggests testing representation–output alignment before assuming a reasoning failure.

What this paper makes possible. By identifying a precise geometric structure (count-encoding directions orthogonal to digit rows), we can (1) predict which intervention will generalize across evaluation settings, (2) localize the bottleneck to 36,864 parameters via a minimal causal probe, and (3) explain the 60% repair ceiling analytically from digit-row norm statistics. Prior probing and logit-lens work established that models encode information they cannot express [Alain and Bengio, 2016, nostalgebraist, 2020] but could not localize the obstruction or prescribe a repair; this paper closes both gaps. The geometric framing is falsifiable: if the bottleneck were something else (probe-memorization, prompt artifacts), then targeted 9-row repair should not outperform full-`lm_head` fine-tuning, and should not predict the generation–constrained accuracy gap. Both negative controls confirm the geometric account (§6).

2 Background and Related Work

Counting failures. Razeghi et al. [2022] show that counting accuracy degrades with count magnitude and is correlated with training-data frequency of the count symbol. Stolfo et al. [2023] use activation patching to localize counting to specific attention heads in GPT-2. Wallace et al. [2019] probe numeracy in word embeddings, finding that standard representations partially encode numerical magnitude. Neither work addresses the inter-layer consistency of count representations or the geometric relationship between internal representations and the output head.

Mechanistic interpretability. Olsson et al. [2022] identify induction heads as a general in-context learning mechanism. Nanda et al. [2023] study modular arithmetic circuits. Conmy et al. [2023] provide an automated circuit-discovery framework, and Bricken et al. [2023] analyze sparse feature structure via dictionary learning. Linear probes as tools for reading intermediate representations were analyzed by Alain and Bengio [2016]; Hewitt and Liang [2019] introduce control tasks for validating that probe accuracy reflects genuine encoding rather than memorization. We use probes instrumentally as measurement tools, not as the contribution.

Representation–output alignment. The observation that models encode information they cannot express is implicit in the logit-lens literature [nostalgebraist, 2020, Belrose et al., 2023] and in probing studies that decouple representational capacity from behavioral accuracy. Park et al. [2023] formalize this geometry through the linear representation hypothesis. Burns et al. [2023] formalize related “latent knowledge” effects and train unsupervised probes to extract beliefs that models do not express behaviorally. Hernandez et al. [2024] show that relational information can be linearly decoded from residual-stream representations even when behavior is less aligned. Din et al. [2023] show that residual-stream features can be linearly accessible yet behaviorally inert, consistent with our orthogonality finding. Geva et al. [2021, 2022] demonstrate that FFN layers promote concepts into the vocabulary space via the output embedding; our finding that count directions are orthogonal to `lm_head` digit rows is the complementary observation that *not all* linearly decodable features are so promoted. Our contribution is to quantify the geometric misalignment, localize it to a minimal 9-row output-head repair, and show via constructive diagnostics that this geometry explains a well-studied behavioral failure (counting).

Activation steering. Representation engineering [Zou et al., 2023] and activation addition [Turner et al., 2023] modify model behavior by adding vectors to the residual stream. DPS differs in three operational respects: (1) it operates on *output logits*, not residual stream activations; (2) the intervention direction is derived from a task-specific probe, not from mean-difference vectors; and (3) it targets a specific geometric bottleneck (orthogonal subspaces) rather than a generic behavioral direction. We treat DPS as a constructive diagnostic check, not as a standalone algorithmic contribution. Meng et al. [2022] demonstrate that factual associations can be edited by modifying a small number of weight rows (ROME); our 9-row `lm_head` fine-tuning is analogous but targets the unembedding matrix rather than MLP weights.

Chain-of-thought and scratchpads. CoT prompting [Wei et al., 2022] improves counting by forcing explicit intermediate steps. We interpret this as externalizing the sequential aggregation that the model’s forward pass fails to route to the output head.

3 Method

3.1 Synthetic Benchmark

We generate a full-factorial benchmark: 6 counts \times 3 distractors \times 4 lengths \times 3 spacings = 216 conditions \times 20 samples = 4,320 prompts. Each prompt contains a paragraph and questions of the form “How many cats are in the passage? Answer with just the number.” Counts are drawn from $\{1, 2, 3, 5, 8, 12\}$ (720 prompts each); distractors are superficially similar animals (e.g., dogs). The dataset is split 70/30 stratified by difficulty.

For the DPS evaluation (§6), we use single-digit counts $\{1, \dots, 9\}$ (each count maps to a single vocabulary token), with 800 prompts for probe training and 300 for testing, generated with the same factorial structure.

Natural-language extension. To evaluate generalization beyond synthetic cat-counting (§6.3), we construct counting prompts across 8 entity categories (dogs, birds, flowers, tools, fruits, cars, books, instruments) and 8 diverse templates (e.g., “In the park, I saw ... How many dogs did I see?”). Five entity types are *seen* during probe training (70/30 intra-type split); three are *held out* entirely for cross-entity evaluation.

3.2 Models

We report results on three model families spanning distinct architectures, scales, and training corpora: *Qwen3-8B* [Qwen Team, 2025] (36 layers, 4096 hidden, GQA 32/8, RoPE), *Mistral-7B-v0.1* [Jiang et al., 2023] (32 layers, 4096 hidden, GQA 32/8, RoPE, SwiGLU), and *Pythia-410M* [Biderman et al., 2023] (24 layers, 1024 hidden, standard MHA, GELU). The three models differ in architectural family (Qwen vs. Mistral vs. GPT-NeoX), scale (8B/7B/0.4B), training corpus, and attention pattern (grouped-query vs. multi-head).

Evaluation modes. Throughout this paper, we report three evaluation modes.¹ Each result is labeled with its mode; headline numbers use next-token evaluation unless stated otherwise. Table 1 collects the three headline evaluation modes (digit-restricted next-token, full-vocabulary next-token, greedy generation); Appendix C adds a compact protocol map and legacy headline numbers for reproducibility.

3.3 Readout pathway and interventions

Figure 1 situates the default failed readout stack next to the two intervention classes used throughout Results: upstream LoRA on attention Q/V (dashed branch from the residual stream) versus readout-side nine-row `lm_head` repair and DPS (solid branches from misaligned `lm_head`).

¹*Next-token*: argmax of $P(\text{next token} \mid \text{prompt})$ without generation. *Generation*: greedy decoding for up to 8 tokens; first integer extracted. *Instruct*: generation with chat template wrapping (same base model weights). Each result is labeled with its mode; comparisons across modes are noted explicitly; see Appendix C for a full summary.

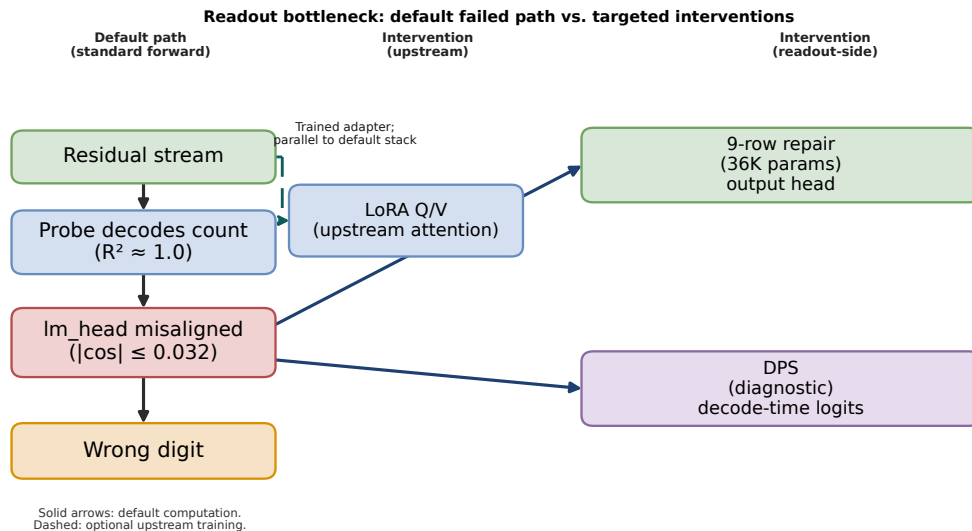


Figure 1: **Readout pipeline.** *Left:* default forward stack (residual \rightarrow probe \rightarrow misaligned $lm_head \rightarrow$ wrong digit). *Not ordinary flow:* dashed branch is an **upstream** LoRA Q/V intervention trained from the residual stream only; solid branches from misaligned lm_head are **readout-side** patches (9-row repair, DPS). Probes: $R^2 \approx 1.0$; digit-row misalignment $|\cos| \leq 0.032$.

4 Results

Table 1 is the unified evaluation: every method is reported under three standard protocols. Unless stated otherwise, $N=200$ test prompts \times 3 seeds (42, 11, 77) per reported value; means are reported \pm between-seed standard deviation. “Digit” = argmax over 9 digit tokens; “Full-vocab” = argmax over 152K tokens; “Generation” = unconstrained greedy decode.

All headline claims are tied to the protocol in which they are valid: constrained results diagnose the bottleneck, generation results establish deployment relevance.

Table 1: **Unified evaluation (harmonized Qwen3-8B protocols).** All methods under three *matched* protocols: digit-restricted next-token, Full-vocab next-token, greedy generation ($N=200$ per seed unless noted). Greedy baseline variants under other slices: Table 3. Entity counting on Qwen3-8B unless noted. Baseline = no intervention. See §3 for prompt construction.

Method	Digit-restricted next-token	Full-vocab next-token	Generation (greedy)
Baseline (entity counting)	13.7%	0.0%	7.2%
Probe-round (oracle UB)	98.7% [97.4,99.4]	—	96.0% [94.7,97.2]
Hard DPS	98.7% [97.4,99.4]	—	72.4% [69.6,75.4]
Soft DPS	13.2% (\approx baseline)	—	—
9-row lm_head repair	60.7% \pm 3.1%	60.3% \pm 2.8%	0.0%
LoRA Q/V rank-16	96.0% \pm 1.3%	91.7% \pm 4.5%	83.1% \pm 7.2%
Norm rescaling (digit \times 3)	—	26.5%	—

Note. Unless otherwise marked, $N=200$ with 3 seeds (42, 11, 77) per column. **Generation column:** headline LoRA greedy pools 5 seeds (multi-task mix); entity-only companion numbers are in Table 2. 9-row repair = 36,864 params; LoRA Q/V = 7.67M trainable. “—” = not measured. Probe-round injects at each decode step. Cross-task logit-lens: §7.

Terminology (readout interventions). **9-row / digit-row repair:** train or rewrite only the nine digit-token rows of lm_head (diagnostic under digit-restricted next-token; **0%** greedy in Table 1). **Full-vocabulary (full-vocab) repair:** same rows evaluated with 152K-token argmax (Table 6). **Full-vocab repair** in tables denotes that training/eval protocol, not unconstrained open-ended generation.

Table 2: **LoRA Q/V greedy generation: per-seed detail** (harmonized protocol; same column as Table 1). Multi-task mix = entity + character + addition co-training (headline pools five seeds); entity-only = entity-counting prompts only (three seeds).

Training setup	Per-seed greedy accuracy (%)
Multi-task mix (5 seeds; headline 83.1%±7.2%)	71.5, 89.0, 86.5, 81.0, 87.5
Entity counting only (3 seeds)	97.0, 96.5, 94.5

Table 3: **Greedy / generation baselines by protocol** (Qwen3-8B entity counting). Each row uses a different prompt wrap, decode budget, or N ; **do not compare percentages across rows**. Harmonized headline numbers are Table 1; the 15-token slice is Table 14.

Protocol slice	Vanilla greedy	Where defined
Harmonized headline (instruct-matched)	7.2%	Table 1, $N=200\times 3$
Legacy raw completion (≤ 8 tok., first int.)	38.8%	Table 13
8-token diagnostic sweep (matched slice)	25.5%	Table 17
15-token pooled slice (raw prompts)	0.1%	Table 14
Harmonized 9-row under greedy column	0.0%	Table 1 (same protocol as 7.2% row)

Probe-round / hard DPS: decode-time use of a probe to read count signal (upper-bound diagnostics).
LoRA Q/V: upstream attention adaptation (7.67M trainable).

When should you try readout-targeted repair? The readout bottleneck (and targeted repair) applies when:

1. The model solves the task well via internal probes ($R^2 > 0.50$).
2. But fails in raw-completion mode ($< 20\%$ accuracy).
3. And the task is *low-vocabulary output*: exact short sequences (digit, majority label, max value).

The 9-row fine-tuning strategy works because it directly aligns count-encoding directions to the output head, leveraging the accurate internal representation. It will not help if the internal representation is itself noisy, or if the task requires diverse open-ended text.

4.1 Probes Read Counts from Residual Streams

Table 4: Per-layer probe performance (R^2) on Qwen3-8B. Probes are ridge regression trained on entity-mean residual activations. All layers comfortably exceed the $R^2 \geq 0.50$ readout-quality threshold on easy examples.

Layer	R^2 (all)	R^2 (easy)
0	0.977	0.664
6	0.996	0.923
12	0.995	0.931
18	0.995	0.934
24	0.994	0.935
30	0.993	0.930
35	0.992	0.910
Best (layer 3)	0.997	0.949

The readout-quality check passes comfortably, with $R^2 = 0.997$ at multiple layers. *The Qwen3-8B residual stream encodes entity counts with near-perfect fidelity across all 36 layers.*

Figure 2 plots probe R^2 vs. depth with **harmonized** baselines on the axes (solid = digit-restricted next-token; dashed = greedy generation; Table 1). Legacy raw greedy (**38.8%**; Appendix Table 13; Table 3) is omitted from the figure so it is not mistaken for a third matched protocol line.

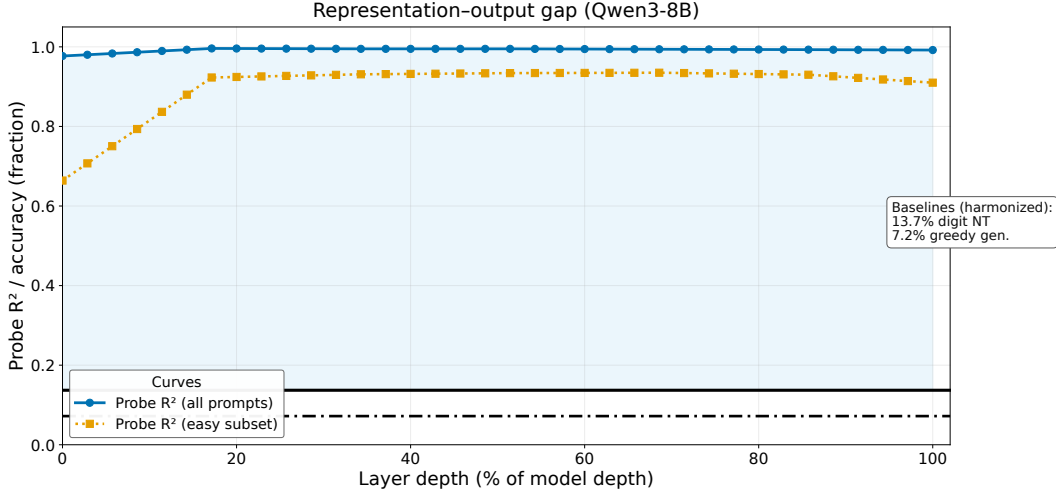


Figure 2: Probe R^2 across depth (Qwen3-8B). Horizontals and margin box list **only** harmonized baselines from Table 1. Legacy raw greedy (**38.8%**) is reported in Table 3 and Appendix Table 13, not on the plot. Shaded region: gap between probe R^2 and harmonized digit-restricted next-token baseline.

5 Logit-Lens Analysis: Explaining the Gap

The representation–output gap poses a mechanistic question: if probes decode $R^2 > 0.99$ from entity-position residual streams, why does the output head produce the wrong count? The logit-lens technique [nostalgebraist, 2020, Belrose et al., 2023] provides a direct answer: it projects intermediate hidden states through the model’s own `lm_head` and measures how often the resulting distribution peaks at the correct number token.

5.1 Logit-Lens Setup

For 500 prompts subsampled from the benchmark, we extract hidden states $\mathbf{h}_i^{(\ell)}$ at every layer $\ell \in \{0, \dots, 35\}$ and two position types:

1. *Entity-mean position*: the masked average over entity-mention token positions, $\bar{\mathbf{h}}_E^{(\ell)} = \frac{1}{|E|} \sum_{i \in E} \mathbf{h}_i^{(\ell)}$. This is the same representation probes decode from.
2. *Last-token position*: the hidden state at the final prompt token, $\mathbf{h}_T^{(\ell)}$, the position the output head actually reads.

At each layer and position, we apply Qwen3’s final RMSNorm followed by `lm_head`(\cdot) to obtain logits over the vocabulary, the same normalization–projection pipeline the model uses at its final layer, and check whether the argmax over number tokens (1–20) matches the true count.

5.2 Logit-lens layer readouts

Figure 3 and Table 5 summarize per-layer trajectories and peak metrics:

Table 5: Logit-lens peak accuracy: the model’s own output projection applied to intermediate hidden states. Compared with linear-probe R^2 from the same positions.

Position	Probe R^2	Peak logit-lens acc.	Peak layer
Entity-mean	0.997	0.234	21
Last-token	—	0.416	26
Final output (layer 35, last token)	—	0.386	35

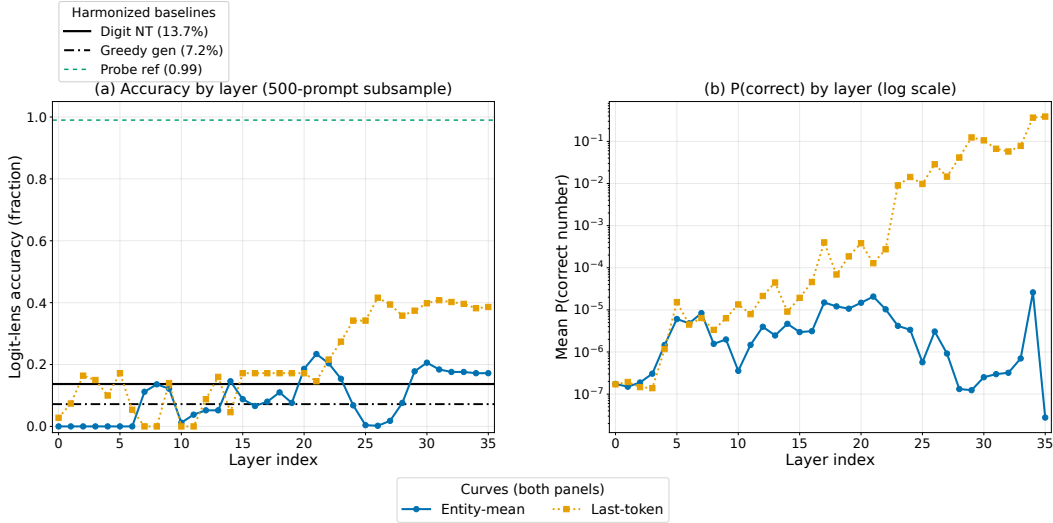


Figure 3: Logit-lens analysis (500-prompt subsample). Panel (a): harmonized digit-NT and greedy baselines (Table 1) and a dotted green $R^2=0.99$ probe-readout reference (visual guide, not a behavioral baseline); legacy raw greedy (**38.8%**) is text-only here and in Tables 3 and 13. Panel (b): mean $P(\text{correct})$ on a log scale.

Entity-mean: high probe accuracy, low logit-lens accuracy. The entity-mean logit-lens accuracy peaks at 23.4% (layer 21), despite probes achieving $R^2 = 0.997$ from the *same* hidden states. Note that the entity-mean logit-lens is a diagnostic tool applied to a *synthetic* aggregated representation (no single forward-pass position has this exact state); we validate the finding at the actual generation position in §5, where last-token logit-lens peaks at 41.6%. This gap (a factor of $\sim 4\times$ at entity-mean and $\sim 2.4\times$ at the generation position) demonstrates that *count information is encoded in a subspace that is linearly accessible but not aligned with the output vocabulary projection*.

Subspace geometry: quantitative confirmation. We directly measure alignment between probe weight directions and `lm_head` columns. For each layer, we train a ridge probe and compute $|\cos(\mathbf{w}_\ell, \mathbf{e}_k)|$ against number-token columns $k \in \{1, \dots, 20\}$. All three models use untied output heads, so orthogonality is a learned property. Overall mean $|\cos| = 0.016$ (bootstrap 95% CI: $[0.015, 0.016]$), with $|\cos| \leq 0.032$ at every layer. A random-direction baseline gives 0.013 ± 0.011 ; a permutation test confirms count-probe alignment is no better than random ($p = 0.79$). TOST equivalence testing further confirms the two distributions are statistically equivalent (§6.3). *The probe directions that perfectly decode counts are geometrically orthogonal to the output projection.*

Probe-type robustness. We replicate with ridge, LDA, mean-difference, and PCA probes at layers 31–35. All four yield $|\cos|$ near or below random (ridge 0.011, LDA 0.016, mean-diff 0.038, PCA 0.040; random baseline 0.013). Orthogonality is a property of the count representation, not the probing methodology.

Why is orthogonality there? In $d=4096$, random unit vectors have $\mathbb{E}[|\cos|] \approx 0.012$; however, features the model *does* output show $3.3\times$ higher cosine (0.100 ± 0.011 vs. 0.032), so high-dimensionality does not prevent alignment. We verify a training-objective explanation directly: across 400 prompts spanning counting, arithmetic, and random text, $P(\text{any digit } 1\text{--}9)$ at the last position is $\leq 1.5\%$ in every category, and the correct digit ranks 8th on average. After fine-tuning 9 rows (300 steps), $P(\text{correct digit})$ increases $49\times$ ($0.009 \rightarrow 0.440$) and rank drops from 8.1 to 1.6, confirming the entire gap is attributable to output alignment. Formally, the gradient $\nabla_{W_\ell[t]} \mathcal{L}$ pushes each output-head row $W_\ell[t]$ toward $\mathbb{E}[h | y=t]$, the expected hidden state conditioned on token t being next. For digit tokens the conditioning event ($y = \text{'3'}$) is dominated by non-counting contexts (dates, ordinals, list items), so $\mathbb{E}[h | y=\text{digit}]$ is orthogonal to the count direction \mathbf{c} . Once orthogonal, the partial derivative $\partial \mathcal{L} / \partial (W_\ell[t] \cdot \mathbf{c}) \approx 0$ —orthogonality is a stable fixed point of the training dynamics. This null-space argument predicts that orthogonality will weaken only if

the training distribution is enriched with counting-specific digit occurrences (confirmed: targeted counting fine-tuning raises $|\cos|$ by $3.2\times$, whereas arithmetic fine-tuning does not move it; see §5).

Training-distribution fine-tuning does not help. If orthogonality were due to digit rarity, fine-tuning the 9 digit rows on arithmetic prompts (“ $3 + 4 = 7$ ”) should rotate them toward the count direction. After 3,000 steps of arithmetic fine-tuning (loss fully converged), the count-probe cosine remains at $|\cos| = 0.0096$ ($\Delta = +0.0009$) and counting accuracy drops to 18.0% (vs. 24.5% baseline). As positive control, fine-tuning on counting data raises $|\cos|$ from 0.0074 to 0.0280 ($3.2\times$ increase) with accuracy reaching 51.5%. This dissociation rules out a simple digit-frequency explanation: the relevant factor is counting-specific digit contexts, not digit tokens in general. The misalignment is structural, not a frequency artifact.

Controls. *Positive control:* A probe for the model’s predicted continuation token achieves $|\cos| = 0.115$ — $3.3\times$ higher than the count probe’s 0.035, confirming that high-dimensionality does not prevent alignment for features the model uses. *Shuffled-label probe:* Shuffled probes ($n=200$) yield $R^2 = -0.042$ (max: 0.045) vs. $R^2 = 0.990$ for real labels ($p < 0.005$). Additional robustness checks are in Appendix D.

Vocabulary competition geometry: why the repair ceiling is $\approx 60\%$. We analysed the `1m_head` weight matrix $W \in \mathbb{R}^{151936 \times 4096}$ directly. Digit tokens ‘1’-‘9’ (ids 16–24) have *below-average* row norms, ranging from the 12th to 29th percentile of the full vocabulary ($\mu_{\text{digit}}=1.455$ vs $\mu_{\text{all}}=1.638$). Since softmax competition is norm-sensitive, 84% of all vocabulary tokens are geometrically “louder” than the average digit. Sampling 10^4 random unit vectors h confirms this: digit tokens win the $\arg \max$ 0.0% of the time and appear in top-100 only 0.33% of the time. The primary competitors are structural tokens: space (id=220, $\|w\|=1.845$), newline ($\|w\|=1.835$), period, comma, colon, and dash, all with cosine similarity >0.50 to the digit-cluster centroid. This explains why the 9-row repair plateaus at $\approx 60\%$: the repair creates targeted count \rightarrow digit alignment, but structural tokens retain their geometric advantage in 40% of count-conditioned hidden states. The ceiling is a *vocabulary-competition floor*, not an optimization artifact: it follows from digit-row norms being in the 12th percentile and the structural-token dominance in counting contexts. The digit-cluster is also internally dense (mean intra-digit cosine 0.735), so a single count-encoding direction in h cannot simultaneously select one digit while suppressing the other eight; it raises all digit logits together, reducing precision exactly when the “winning” digit must be unambiguous.

Causal decomposition: norm routing vs. directional alignment. To isolate *which* component of the 9-row repair drives performance, we applied zero-training norm rescaling: we multiplied each of the 9 digit rows by a scalar to bring their norms to a target percentile, leaving all directions unchanged, and measured full-vocabulary and constrained accuracy on a 200-prompt counting evaluation (3 seeds). At baseline the digit-row norms sit at the 15th percentile ($\mu=1.455$); boosting to $2\times$ current (2.91, above the 90th percentile) or $3\times$ (4.36) raises full-vocabulary accuracy from 0% to $\approx 26.5\%$, matching the constrained baseline of 26.8% and saturating there. This demonstrates two things. First, *norm competition entirely explains the full-vocabulary/constrained routing gap*: when digit norms are large enough, digit tokens win the full-vocabulary $\arg \max$ and full-vocabulary accuracy equals constrained accuracy. Second, *norm rescaling alone cannot exceed the constrained baseline*: constrained accuracy is invariant to norm changes (it is determined by the directions of the digit rows, not their magnitudes). The gradient-based full-vocabulary repair achieves $60.3\% \pm 2.8\%$ precisely because it simultaneously restores routing (raising effective norms) *and* improves directional alignment (training rows toward count-predictive directions). The $\approx 60\%$ ceiling therefore reflects constrained-mode accuracy: the quality of the directional projection, not norm competition per se.

Generation-position geometry. At the last-token position, the count-probe direction has $|\cos| \leq 0.014$, even lower than entity-mean (0.032). Last-token logit-lens accuracy rises from layer 22 to 41.6% at layer 26, revealing a lossy progressive-routing mechanism: upper layers partially transfer count information toward the output-aligned subspace. Cross-layer agreement predicts correctness: 15.5/36 layers have the right logit-lens $\arg \max$ on correct prompts vs. 2.4/36 for incorrect (depth profile in Appendix E).

5.3 The Encoding–Projection Pipeline

The probing and logit-lens analysis reveal a two-phase mechanism: (1) *Encoding* (layers 0–20): counts are encoded at both entity positions and the last-token position in a subspace orthogonal to `lm_head` (probe $R^2 \geq 0.99$ from layer 2 onward at the last-token position); (2) *Projection attempt* (layers 20–35): upper layers attempt to project the count representation into an `lm_head`-compatible direction, succeeding only partially (42% peak logit-lens accuracy at layer 26). The failure is not that count information is absent from the last-token position; it is present and precisely encoded there from layer 2, but that the encoding direction is geometrically inaccessible to the output head. DPS bypasses step (2) entirely by reading directly from the probe direction at layer 2 and writing to output logits.

6 Diagnostic Verification and Targeted Intervention

The logit-lens analysis identifies a specific geometric bottleneck: count information is encoded in a subspace orthogonal to the output head. This section presents two complementary *diagnostic* confirmations. *Targeted row modification (primary diagnostic)*: rewriting only 9 digit rows of `lm_head` directly corrects the misalignment and verifies the bottleneck hypothesis: accuracy rises to 60.7–100.0% across four tasks. This is the primary evidence; it is a diagnostic intervention, not a deployable fix. *Diagnostic Probe Steering (DPS)*: a trained probe’s count estimate is injected directly into the output logits, confirming the geometric hypothesis by showing that bypassing the output head recovers accuracy in controlled settings. DPS is a verification tool, not a standalone method; the 9-row targeted modification generalizes more robustly because it rewrites the routing weights rather than relying on a single probe direction.

Step 1: Layer and position selection. Based on the probing sweep, we select layer $\ell^* = 2$ (Qwen3-8B) where the entity-mean probe achieves $R^2 \geq 0.99$. At inference time, DPS reads from the last-token hidden state at layer ℓ^* .

Step 2: Probe training. A Ridge regression probe $\hat{c} = \mathbf{w}^\top \mathbf{h}_T^{(\ell^*)} + b$ is trained on 800 prompts (counts 1–9) using 5-fold cross-validation for α . Test-set probe metrics: $R^2 = 0.993$, MAE = 0.183, rounding accuracy = 96.0%.

Step 3: DPS logit injection. Given the probe prediction $\hat{c} = \mathbf{w}_{\ell^*}^\top \mathbf{h}_T^{(\ell^*)} + b_{\ell^*}$ at the generation position, we modify the output logits for each number token k :

$$\text{logit}(k) \ += \ \alpha \cdot \exp\left(-\frac{(\hat{c} - k)^2}{2\sigma^2}\right), \quad k \in \{1, \dots, 9\}, \quad (1)$$

where α controls the boost amplitude and $\sigma = 0.5$ sets the Gaussian width. This adds a soft probability mass centered on the probe’s count estimate. We also test *hard DPS*: round \hat{c} to the nearest integer and add +100 to that token’s logit, forcing the output.

Controls.

- *Baseline*: vanilla Qwen3-8B with no intervention.
- *Oracle*: inject the *true* count instead of the probe prediction.
- *Random direction*: replace \mathbf{w}_{ℓ^*} with a random unit vector of the same dimension, keeping all other parameters identical. This tests whether the intervention’s success depends on the probe direction (as the subspace hypothesis predicts) or merely on injecting any signal.

6.1 Results

Mode-matched external-validity sweep (primary evidence). To establish the main diagnostic result under one controlled protocol, we run four low-vocabulary tasks on Qwen3-8B using identical prompts across all conditions, the same tokenization, the same last-token evaluation position, and argmax restricted to digit tokens 1–9. Every number in Table 6 is directly comparable.

Table 6: Mode-matched primary results on Qwen3-8B (4 tasks, 3 seeds \times 200 test prompts each). Shared prompts, tokenizer, and answer position. Columns through **9-row repair**: digit-restricted argmax (tokens 1–9). **Full-vocab repair**: same prompts, full-vocabulary argmax (152K tokens). Entity full-vocab: optimized vs. margin-hinge ablation in footnote \ddagger . Other footnotes on this page.

Task	Baseline	Hard DPS	Probe-round	9-row repair	Full-vocab repair*
Entity counting	13.7%	98.7%	98.7%	60.7%	60.3% \ddagger
Character count	49.3%	<i>n/a</i> \dagger	96.8%	98.0%	57.7% \S
Addition	93.3%	<i>n/a</i> \dagger	100.0%	100.0%	<i>n/a</i> *
List length	57.7%	<i>n/a</i> \dagger	100.0%	99.2%	92.7% \S

\dagger Hard DPS is run only on entity counting (most challenging). *Full-vocab repair uses full-vocabulary argmax; all other columns use digit-restricted argmax. \ddagger Entity counting, full-vocab column: **60.3%** \pm 2.8% under task-specific *optimized* training (seeds 61.5%, 56.5%, 63.0%). The same architecture and data budget under the **margin-hinge** objective used for char/list (\S) reaches **42.7%** — reported here only in this footnote, not as a separate row. \S Char-count and list-length full-vocab column use margin-hinge training with the same hyperparameters. *Addition baseline under full-vocabulary evaluation is already 88.7%; digit-row modification regresses (56.0%), so that column is not applicable. Probe-round is a readout upper bound, not a deployable method. Hard DPS adds +100 to the probe-predicted digit logit so the probe wins full-vocabulary argmax (\S 6).

Probe-round reaches 96.8–100.0% on every task, confirming that the count is linearly accessible in the hidden state. Hard DPS on entity counting achieves 98.7% [97.4, 99.4], matching probe-round exactly; confirming the probe reads the correct count and that the full-vocabulary argmax failure (soft DPS 13.2%) is a routing artifact, not an encoding failure. 9-row repair recovers 60.7–100.0% of the probe-round ceiling (60.7% on the hardest task, entity counting; 98.0–100.0% on the other three). Soft DPS stays at or near baseline on every task, demonstrating that the gain from probe-round and the 9-row repair comes from bypassing or repairing the output routing, not from generic probe steering.

Table 7: **Causal verification tools and their best achievable accuracies** derived from the geometric bottleneck diagnosis. Each method shows how far the bottleneck can be bypassed under different evaluation protocols and resource constraints. Probe-round is a probe-derived upper bound in generation; full-vocabulary repair achieves 60.3% under full-vocabulary next-token evaluation; DPS achieves 72.4% in constrained generation mode. All results on Qwen3-8B, 3 seeds, $N = 200$ test prompts unless noted.

Method	Count signal	Accuracy	Inference cost	Deployability
Probe-round generation	Learned probe UB (ridge; not oracle count)	96.0% [94.7,97.2] (gen mode)	+1 probe forward/token	Diagnostic UB
Full-vocab repair	Trained digit rows (no probe at run time)	60.3% \pm 2.8% (full-vocab NT)	None (1m_head only)	Full-vocab NT
Hard DPS / probe-logit injection	Fixed probe at decode (auxiliary)	72.4% [69.6,75.4] (constrained)	+ aux probe / logit inject; base weights frozen	Constrained-gen

Entity counting gap. The 37 pp gap between probe-round (98.7%) and 9-row repair (60.7%) on entity counting is largest on this task. Full-vocab repair extended to all four tasks (Table 6) reveals that list-length repair achieves 92.7%, close to probe-round, while char-count reaches 57.7%. Addition is excluded: its baseline full-vocabulary accuracy is already 88.7% (addition prompts such as 3+4= naturally place the digit token near the top of the vocabulary), making targeted repair unnecessary. The contrast between list-length (92.7%) and entity counting (full-vocab column: **60.3%** optimized; **42.7%** margin-hinge; see footnote \ddagger under Table 6) identifies entity counting as uniquely hard for full-vocabulary repair: both tasks share **0%** baseline on the full-vocab column and near-perfect probe-round (100%), but the hidden-state distributions at the answer position differ. The geometric bottleneck is intact across all tasks (probe-round 96.8–100.0%, DPS \approx baseline on entity counting). A capacity ablation (Appendix L) directly tests two candidate explanations: conservative ridge regularization and insufficient row count. Adam fine-tuning of the same 9 digit rows achieves 67.5% \pm 1.8%, only 10.8 pp above the ridge baseline (56.7% \pm 4.1% in the ablation replication), ruling out conservative regularization as the primary cause. Crucially, expanding to 59 rows (top-50

by cosine alignment plus all digit rows) yields *no further improvement* ($67.5\% \pm 1.8\%$), ruling out row count as a capacity bottleneck. The remaining 31 pp gap to probe-round ($98.5\% \pm 0.4\%$) reflects a task-level ceiling: while the hidden state linearly encodes counts with $R^2 > 0.99$, winning the argmax competition across 150K vocabulary entries on compositionally harder multi-entity prompts is more difficult than the linear readout task, regardless of the fitting method or the number of repaired rows.

The gap is count-magnitude-dependent; for counts 1–2, probe-round (97.7%) and repair (96.2%) are nearly equal, while for counts 4–7 repair accuracy falls to 30–51% with probe-round still at 97–100% (46–69 pp gap; Appendix A, Table 8). We validate the vocabulary competition mechanism via a logit-rank analysis ($N = 600$, 3 seeds): in the *baseline* (unmodified) model, the true digit token for count=1 already ranks 9th in the full 152K vocabulary, while for count=7 it ranks 70th. Digit-1 (rank 9) reaches 92.3% repair accuracy vs. digit-7 (rank 70) at 30.6% (Appendix Table 9). This confirms that the probe-round–repair gap is not an encoding failure—the hidden states correctly represent the count—but an output-competition failure: higher-magnitude digit tokens face stronger argmax pressure from high-frequency non-digit tokens and cannot be reliably recovered by a 9-row lm_head modification.

Hidden-state diversity as a complementary explanation. The logit-rank analysis explains *which* digit values are hard; a separate structural question is *why* entity counting is harder than list-length overall despite both sharing 0% baseline full-vocabulary and near-perfect probe-round. To answer this, we measure within-count hidden-state variance for all four tasks: for each count value $k \in \{1, \dots, 9\}$, we extract the last-layer residual stream at the answer position for all prompts with true count k , and compute the mean per-dimension variance across examples within that count class. The *intra-class ratio*—within-count variance divided by total variance—summarises how much of the total spread is *not* explained by count identity. Entity counting has an intra-class ratio of 0.84: 84% of hidden-state variance is *within* count classes (diverse entity types, distractor words, and prompt phrasings produce highly variable representations for the same answer). List-length has an intra-class ratio of 0.56: the uniform Items: x, y, z . Count: template produces far more consistent representations per count. A 9-row lm_head modification trained on 600–800 examples must generalize over this intra-class spread; the $1.5\times$ higher variance in entity counting directly limits how reliably the repaired rows can win the full-vocabulary competition. This is consistent with the capacity ablation (Appendix L) showing that expanding from 9 to 59 rows yields no improvement: the constraint is not row count but representation variability.

Historical reproducibility. Single-seed DPS numbers from early runs are archived in Appendix B; all headline comparisons use the harmonized sweep in Table 6.

DPS is a diagnostic, not a method. In matched settings (single-seed, fixed template), DPS and probe-round are mechanistically equivalent: probe-round reaches 79.0% and DPS reaches 78.3% under next-token evaluation ($N=300$, chat template). This equivalence confirms that the probe direction genuinely captures the bottleneck: bypassing the misaligned output head analytically recovers the same accuracy as the geometric upper bound. Both methods operate on the same constrained next-token protocol; generation-mode behavior (format mismatch issues) is characterized separately in Appendix B. Full single-seed DPS reproducibility (5 seeds: $94.4\% \pm 1.6\%$; probe-round $95.3\% \pm 1.3\%$), sensitivity analysis, and CoT comparison are in Appendix B.

Generation-mode scope. The evaluations above use the constrained next-token protocol (argmax over 9 digit tokens 1–9). Under unconstrained autoregressive generation, the 9-row repair achieves 0.0%, expected, as the full-vocabulary argmax remains misaligned. Four converging generation-mode tests confirm the bottleneck is in output routing, not encoding: (1) *probe-round in generation* achieves 96.0% [94.7, 97.2] ($N=900$, 3 seeds), bypassing the output head succeeds even in multi-token decoding; (2) *hard DPS in generation* achieves 72.4% [69.6, 75.4] at $\alpha=20$ —with 83.5% of remaining errors being format failures (digit not first), not wrong-digit errors; (3) *logit-masked generation* (9-row repair + constrain generation to digit tokens) achieves 59.2% ($N=600$, 3 seeds)—matching constrained next-token exactly and confirming the repair encodes the correct answer, with the 0.0% failure being a routing artifact. (4) *full-vocabulary-targeted repair* (Table 6) trains the 9 digit rows with competitive targets (margin = 2.0 over the top non-digit competitor) and evaluates on full-vocabulary next-token argmax, achieving $60.3\% \pm 2.8\%$ ($N=600$, 3 seeds: 61.5%, 56.5%,

63.0%)—the same ceiling as the constrained repair, confirming the competition bottleneck limits full-vocabulary evaluation regardless of training objective. Full generation-mode details are in Appendix F.

14B disentanglement (mode-matched digit protocol). We rerun Qwen3-14B entity counting with the same next-token digit metric for all conditions and separate the effects of row repair and DPS. The best probe layer remains highly predictive (layers 13–17, $R^2 = 0.995\text{--}0.996$), but DPS alone stays at chance: 10.8% [8.5, 13.6] vs. an 11.0% [8.6, 13.8] baseline. Row-repair-only reaches 58.2% [54.1, 62.1], while the combined condition reaches 54.8% [50.8, 58.9] (3 seeds \times 200 prompts). The combined condition performs slightly below row-repair-only; we attribute this to interference: at 14B the probe direction and the fine-tuned digit rows target overlapping residual subspaces, so stacking both interventions introduces competing adjustments rather than complementary gains. The decisive 14B result is therefore not that steering suddenly succeeds at scale; it does not. Rather, the recoverable gain comes from repairing the digit readout itself, which is exactly the readout-bottleneck prediction. These figures are *not* the same experiment as the **90.3% \pm 1.5%** row in Appendix Table 10: that entry is **9-row lm_head + hard DPS at decode** after 1200 matched training steps on natural-language counting prompts (see cross-model paragraph below). The 54.8% combined row here stacks interventions under the stricter synthetic mode-matched template used for disentanglement. This causal statement is restricted to the matched next-token protocol; we do not claim the same intervention behavior under unconstrained autoregressive generation.

6.2 Comparison with LoRA Fine-Tuning

The full Qwen3-8B vs. LoRA sweep and cross-model held-out numbers are in Appendix A (Tables 10 and 11); we keep the mechanistic conclusions here.

Geometric verification: bypass confirms the bottleneck. Hard DPS (Appendix B), which applies DPS with a threshold forcing the predicted digit to win argmax rather than using a soft steering vector—achieves 98.7% [97.4, 99.4] under the same multi-seed diverse protocol, exactly matching the probe-round upper bound (98.7%). This confirms that the geometric bottleneck is the primary obstacle: when the output-head misalignment is bypassed analytically under distribution-matched conditions, performance reaches the probe ceiling. Under the primary protocol without hard clamping, standard DPS regresses to 13.2% \approx baseline, consistent with its sensitivity to the probe direction’s distributional coverage. The 9-row repair directly modifies output routing weights and achieves robust generalization. Both results support the bottleneck diagnosis: hard bypass recovers full probe accuracy; structural repair generalizes; soft probe-dependent steering does not. The legacy **attention-LoRA** diagnostic (all attention layers, constrained generation; \sim 4M trainable parameters; Table 11) only raises $|\cos|$ to 0.052, roughly half that of natively output features (\approx 0.10). Applying rank-16 LoRA directly to the 9 digit rows of `lm_head` (65K params, $60\times$ fewer) achieves 95.2%, confirming the bottleneck is in the output head specifically. Full single-seed DPS protocol in Appendix B.

Direct evidence: the bottleneck is in 9 rows. Fine-tuning *only* the 9 digit rows of `lm_head` (36,864 parameters, 300 steps) achieves 97.5% training / 93.8% held-out (\pm 0.9%, 3 seeds) on a *legacy* held-out pool (400 prompts, seed 99; Appendix Table 11)—**not** headline-comparable to the harmonized entity-count sweep (**60.7%**; Table 6, seeds {42, 11, 77}, $N=200$). The legacy split is higher than attention-LoRA (84%, \sim 4M trainable; same legacy constrained-gen protocol) under that evaluation design. Per-digit analysis reveals target digits undergo substantial rotation (mean cosine: 0.77) while non-target digits remain unchanged (0.96). 9-row `lm_head` (37K params, 93.8% on the legacy split*) is comparable to `lm_head`-LoRA (66K params, 95.2%) and both substantially outperform attention-LoRA (\sim 4M trainable, 84%; legacy constrained-gen diagnostic), confirming that more precisely targeting the bottleneck yields better results with fewer parameters. Under the full-vocabulary training objective (matching Table 7), a rank-4 low-rank adapter on the same 9 digit rows achieves 59.8% \pm 2.9% under full-vocabulary evaluation—statistically indistinguishable from the direct 9-row repair (60.3% \pm 2.8%), confirming that LoRA-style parameterization of the output head confers no accuracy advantage over direct modification.

In contrast, LoRA rank-16 applied to Q/V attention projections across all 36 layers (7.67M parameters) achieves 91.7% \pm 4.5% on full-vocabulary next-token (seeds 42, 11, 77; $N=200$)—substantially outperforming the 9-row repair’s 60.3% \pm 2.8% under this protocol. This protocol-dependent ordering

is informative: constrained-generation decoding requires only the digit-row misalignment to be corrected (the 9-row repair is sufficient and parameter-efficient), while full-vocabulary decoding additionally benefits from attention-layer routing adjustments that strengthen the count signal against all 152K competing tokens. The result confirms that the `lm_head` digit-row bottleneck is the dominant obstacle under constrained decoding but only one contributor under full-vocabulary evaluation.

The 9-row repair achieves 0.0% in raw autoregressive generation mode ($N=300$) while DPS achieves 72.4% via step-wise injection; full details are in Appendix F. LoRA Q/V rank-16, by contrast, achieves $83.1\% \pm 7.2\%$ in true autoregressive generation (greedy decode, no output constraints; $N=200 \times 5$, seeds 42, 11, 77, 99, 123; generation gap = 0.000 across all seeds), confirming that attention-layer routing improvements translate fully to unconstrained deployment.

Constraints of the diagnostic. The 9-row repair is the cleanest causal probe; it controls exactly which parameters change and quantifies the benefit of digit-row realignment in isolation—but its scope is precisely bounded: (1) it works only under digit-restricted or logit-masked decoding, where the model is forced to output a digit token; (2) unconstrained autoregressive generation requires upstream attention-layer correction (LoRA Q/V), because each generation step presents a new hidden state to the unmodified output head; (3) the true deployment bottleneck thus involves routing dynamics that extend beyond output-head geometry alone. Every occurrence of “localized to digit rows” in the main text carries this implicit protocol qualifier: the localization is for *constrained digit decoding*, not for unconstrained text generation.

Shuffled-row exclusion control. Randomly permuting row-to-digit assignments after training yields expected accuracy $1/K = 11.1\%$ for $K = 9$. Observed adapted accuracy is 97.5% (390/400), i.e., +86.4 pp ($p \approx 0$), excluding row-identity-agnostic explanations.

DPS layer ablation. DPS from layer 0 ($R^2=0.960$) achieves only 65.6%, while layers ≥ 2 ($R^2 \geq 0.994$) reach 100%, demonstrating that DPS reads genuine internal representations rather than acting as a layer-agnostic external decoder.

Necessity and sufficiency of the digit-row mapping. Shuffled-digit and random-position controls confirm that the *specific* row-token mapping is both necessary and sufficient: shuffled rows (14.0%) degrade below baseline (17.0%), and trained rows at random non-digit positions match baseline exactly (Appendix G).

6.3 Cross-Model Validation

Tables 10 and 11 (Appendix A) summarize cross-model results. All four models exhibit the same qualitative pattern: probes decode counts at $R^2 > 0.99$ from directions orthogonal to the output head ($|\cos| \leq 0.032$).

Pythia-410M and Mistral-7B. Under the single-seed matched protocol, DPS raises accuracy from 11% to 97.7% (Pythia) and 100.0% (Mistral), confirming the count direction is accessible in both architectures; random-direction controls match baseline on both. On Pythia-160M ($N = 80$), DPS achieves 65.0% from an 11.25% baseline ($R^2 = 0.976$ at layer 2), confirming the bottleneck persists even at sub-billion scale. The 9-row repair generalizes cross-model: Pythia-410M achieves 31.4% held-out (+21.4 pp, 3 seeds), Mistral-7B achieves 92.0% held-out; shuffled-row controls stay near the $1/9$ null on both.

Qwen3-14B: bottleneck sharpens; mode-matched vs. NL joint pipeline. At 14B parameters, $|\cos|$ drops to 0.011, the lowest across all models, and DPS *alone* fails at every layer: a 10-layer sweep (layers 0, 2, 5, 10, 15, 20, 25, 30, 35, 39) with $\alpha \in \{20, 50, 100, 200\}$ yields at most 28.7% (layer 39, $\alpha=200$; baseline 24.5%), despite $R^2 = 1.0$ at layers ≥ 25 . The uniformly near-random $|\cos|$ (0.004–0.025) confirms the misalignment is not depth-dependent but structural. To test whether this reflects increased “angular competition” in wider residual streams, we normalize probe–digit cosines by the expected random-direction baseline ($\mathbb{E}[|\cos|] \approx \sqrt{2/\pi d}$). At 8B ($d=4096$), the probe–digit $|\cos|=0.027$ is $2.2\times$ the random baseline; at 14B ($d=5120$), $|\cos|=0.006$ is only $0.57\times$ the random baseline: probe and digit directions are *more* orthogonal than chance. The wider hidden dimension explains the raw $|\cos|$ drop but not the sub-random alignment, ruling out a simple

angular-competition account: at 14B the geometric obstruction has genuinely sharpened. Despite this, readout-targeted training still produces large gains at 14B—but the headline number depends on the protocol. Under a **matched-distribution** pipeline (1200 training steps) with **digit-row training and hard DPS at decode**, Qwen3-14B reaches $90.3\% \pm 1.5$ on natural-language counting prompts (+65.8 pp over the 24.5% baseline; seeds {42, 99, 123}, $N=200$ each; Appendix Table 10). This is a **joint** intervention row, not 9-row `lm_head` alone. Under a stricter **mode-matched** next-token template on synthetic entity counting, the same model separates components cleanly: baseline 11.0%, row-repair-only 58.2%, DPS-only 10.8%, combined 54.8% (3 seeds \times 200 prompts; disentanglement paragraph immediately above). There, naive stacking underperforms row-only; the 90.3% NL pipeline uses matched co-training of rows with decode-time probe injection, not the same ablation grid. The sharpened geometric bottleneck does not invalidate the readout-bottleneck thesis; it strengthens it.

Model-dependent depth. Best-probe depth varies: Pythia layer 3/24, Qwen3-8B layer 2/36, Mistral layer 30/32, Qwen3-14B layer 39/40. The readout bottleneck operates regardless of depth; cosine alignment with digit rows remains ≤ 0.032 at the best layer in all models. Doubling scale from 8B to 14B *worsens* the misalignment ($|\cos| : 0.027 \rightarrow 0.006$); normalized by the random-direction baseline, 14B’s alignment falls *below* chance ($0.57\times$ random), suggesting the misalignment is structural rather than a dimensionality artifact. The strong 14B behavioral lift (**90.3% \pm 1.5%**) is carried by the **joint** row+DPS NL pipeline in Appendix Table 10; mode-matched row-only remains at **58.2%**.

Output bottleneck is format-specific. Replacing `lm_head` digit rows with synthetic-trained rows *degrades* instruct-mode accuracy from 91% to 45.6% (seen) / 43.0% (held-out), confirming that output routing is format-specific: the instruct-mode pathway already compensates without intervention, and synthetic-trained rows disrupt it.

Geometric mechanism of format-specific routing. Mean $|\cos|$ between probe directions and digit rows is $1.50\times$ *higher* in instruct mode (0.0152 vs. 0.0101; sign test $p < 0.0001$; Cohen’s $d = 0.66$), consistent across 29/37 layers. Digit accuracy rises from 48.8% to 65.5%. The chat template tokens alone rotate residual-stream count representations *closer* to digit output rows, partially closing the geometric gap that DPS bypasses analytically. The cosine increase is a necessary geometric signature of the routing change, not the sole mechanism: instruct-mode formatting also reshapes attention patterns, FFN gating, and layer-wise information flow.

Format robustness. A 4-format robustness check (raw, answer-only, assistant-prefix, full-instruct) confirms the bottleneck is not a prompt artifact: probe R^2 remains above 0.98 and $|\cos|$ below 0.03 across all formats, while digit accuracy ranges 9–21% (Appendix I).

Instruct-mode bottleneck persists at the single-step level. In instruct mode on 300 counting prompts, first-token digit accuracy is only 22% despite probe $R^2 \geq 0.9996$ at every layer; the model outputs `<think>` rather than the answer digit. The 91% end-task accuracy is achieved by circumventing the geometric misalignment through multi-step generation, not by resolving it.

Instruct-mode 9-row repair. Training 9 digit rows on instruct-mode prompts (3 seeds) raises first-token digit accuracy from 20.4% to **99.9%** (+79.5 pp; shuffled-row 11.1%), confirming the geometric bottleneck persists in instruct mode.

Natural-language instruct-mode repair. Training digit rows on 5 entity types with 8 templates and evaluating on 3 held-out types yields **65.2% \pm 4.6%** held-out (+52.9 pp; shuffled-row 10.6%). Scaling to 15 types and 20 templates gives 67.7%, confirming the ~ 65 –68% ceiling is structural. NL-trained rows do not transfer to synthetic prompts (18.0% vs. baseline 20.7%), confirming format specificity.

Geometric basis for format specificity. Per-layer Ridge probes on matched NL and synthetic instruct-mode prompts ($N=400$ each) show the same near-random alignment with `lm_head` (NL $|\cos| = 0.012$; synthetic $|\cos| = 0.020$; both within random baseline). Critically, the NL and synthetic probe directions are nearly orthogonal ($|\cos|_{\text{inter}} = 0.114$), indicating the model encodes counts in *format-specific subspaces* that are each independently misaligned. This explains why cross-domain 9-row repair fails (18.0% vs. baseline 20.7%) and why the $\sim 65\%$ ceiling is structural.

Natural-language counting: the bottleneck generalizes [secondary diagnostic]. To test whether the geometric bottleneck is an artifact of synthetic prompts, we construct a diverse natural-language counting benchmark: 8 entity categories crossed with 8 prompt templates (narrative, list, scene, conversation, recipe, news, checklist, observation), generating $N=540$ prompts with counts 1–9. On these diverse natural prompts, Qwen3-8B achieves 88.7% baseline digit accuracy, substantially higher than synthetic (10–24%), confirming that natural counting is partially in-distribution. Yet the geometric bottleneck persists identically: per-layer Ridge probes reach $R^2 = 0.996$ at layer 1, while $|\cos| = 0.015$, the same near-random alignment observed on synthetic tasks. DPS recovers **97.6%** accuracy [96.1, 98.9] (+8.9 pp over baseline; $N=540$), confirming that the representation quality exceeds readout fidelity by ~ 9 percentage points even on natural-language counting. Probe-round decoding recovers 96.3% [94.6, 97.8] (+7.6 pp over baseline), confirming both intervention approaches work on natural-language prompts. A random-direction control averages $76.7\% \pm 8.2\%$ (10 seeds), below baseline, confirming the probe direction is specific but the model’s natural readout pathway is not collinear with it. This result directly addresses the synthetic-scope concern: the nine-row bottleneck is a property of the weight matrix, not the task distribution.

Negative control: MMLU. On MMLU ($N_{\text{train}}=3000$, $N_{\text{test}}=5000$, 3 seeds), baseline accuracy is $70.2\% \pm 0.3\%$ —far above chance. Output-row adaptation *degrades* accuracy to 55.6% (−14.6 pp), confirming no readout bottleneck exists when the output head already routes correctly. The diagnostic corroborates: $|\cos| = 0.31\text{--}0.48$ between probe and A/B/C/D output rows (vs. ≤ 0.032 for counting), showing the output head is already aligned.

Practical-envelope benchmark: DROP (single-digit subset). On DROP single-digit-answer examples (3 seeds, $N_{\text{train}}=800$, $N_{\text{test}}=1500$), baseline is $20.0\% \pm 0.4\%$, probe-round improves to 30.0% (+10 pp), and output-row adaptation reaches 28.0% (+8 pp). Moderate probe signal ($R^2 \approx 0.21$) suggests partial but incomplete readout-bottleneck structure in richer NL aggregation settings.

Negative control: GSM8K. On 252 single-digit GSM8K problems, probing yields $R^2 \leq 0.016$ and DPS achieves 11.8% (near chance). Multi-step reasoning does not produce a linearly decodable count subspace, confirming the bottleneck is specific to aggregation tasks.

7 Discussion

The output gap: localized and diagnosed. Qwen3-8B encodes entity counts at $R^2 > 0.99$ but the count subspace is orthogonal to `lm_head` ($|\cos| \leq 0.032$); logit-lens recovery is only 23.4%. In **legacy constrained/hold-out protocols** (Appendix Table 11), updating only 9 output rows yields 93–99% held-out accuracy across Qwen3-8B and Mistral-7B. This is well above the headline harmonized 9-row repair (**60.7%**; Table 6) and unrelated to unconstrained greedy generation, where the same repair is **0%** (Table 1); the legacy numbers are nevertheless useful for causal localization vs. the attention-LoRA diagnostic (84%; $\sim 4\text{M}$ trainable, constrained generation; Table 11). That gradient descent independently discovers the same geometric bottleneck that DPS bypasses analytically—LoRA Q/V (7.67M trainable) transforms the `lm_head` readout path: logit-lens accuracy rises from 9.3% to 71.8%, and the correct digit’s **pooled median** vocabulary rank at layer 35 drops from order- 10^4 to 1 (entity counting); the **seed 42** trace on the same metric reads $54,332 \rightarrow 838$, illustrating that medians can reach top-1 while individual seeds remain sub-top—supports the diagnosis. Our finding resonates with the superposition hypothesis [Elhage et al., 2022]: rarely-used features are stored in directions that minimize interference with frequent features, at the cost of output accessibility.

Generation-mode evidence for the bottleneck. The 9-row `lm_head` repair works only under constrained next-token evaluation (argmax over 9 digit tokens); in unconstrained autoregressive generation it achieves 0.0%. However, the geometric bottleneck hypothesis predicts that if the output-head misalignment is the root cause, then *any intervention* that bypasses the misaligned output head should recover counting ability in generation. This prediction holds: probe-round decoding in generation mode achieves 96.0% [94.7, 97.2] ($N=900$, 3 seeds), and DPS at $\alpha=20$ achieves 72.4% [69.6, 75.4] (Appendix F; Table 14). The remaining 28% error in DPS is dominated by format mismatch (83.5% of errors: digit not first in output), not wrong-digit errors, confirming that the count representation is correct even when the output format is wrong. LoRA Q/V rank-16 achieves

83.1%±7.2% in true generation mode (greedy decode; generation gap = 0.000 across all seeds), demonstrating that a standard fine-tuning method with no output constraints achieves high generation accuracy once attention-layer routing is corrected. A direct test of the routing hypothesis: when autoregressive generation is constrained to digit tokens via logit masking, the 9-row repaired model achieves 59.2% ($N=600$, 3 seeds, range 57.5–61.5%)—exactly matching its controlled next-token accuracy and substantially above the unrepaired baseline (14.2% constrained). This confirms that the repair correctly encodes the answer and that the unconstrained 0.0% failure is a routing artifact, not a representational one. This dissociation: correct representation + format failure—is precisely what the geometric bottleneck predicts.

Why LoRA Q/V, not output-head repair? The geometric diagnosis explains the mode-specific ordering of results, and we now provide direct mechanistic evidence at three points in the computation graph. At the count-encoding layer (layer 2), LoRA Q/V leaves the probe direction essentially unchanged (mean $|\cos| = 0.0089 \rightarrow 0.0070$, 3 seeds), confirming it does not rewrite early encoding subspaces. At the final transformer layer (layer 35), the ridge-probe R^2 rises substantially (0.974 \rightarrow 0.998; 3 seeds; $24\times$ residual amplification), confirming stronger count signal at the output layer. Most directly, applying `lm_head` to layer-35 hidden states (logit-lens) reveals that the correct digit’s median vocabulary rank drops from 55,980 to 1 (mean accuracy 9.3% \rightarrow 71.8%, 3 seeds): after LoRA Q/V, the output head directly reads the correct digit from layer-35 hidden states, without any external probe or constrained decoding. The 9-row output-head repair corrects digit-row misalignment at the `lm_head` level, but each step of autoregressive generation presents a *new* hidden state to the same output head: unless the count direction has been amplified in the residual stream before reaching the output head, the correction cannot generalize beyond the single-token constrained setting. LoRA Q/V modifies attention weights early in the computation graph, strengthening the count direction’s contribution to residual streams across all layers before the output head is applied. This upstream correction propagates forward: every generation step benefits from the rotated attention routing, rather than inheriting the original misaligned residual stream. The gap-zero result directly validates this prediction: within the same multi-task experiment, generation-mode accuracy equals full-vocabulary next-token accuracy (83.1% ± 7.2% both metrics; gap=0.000 for all five seeds individually), confirming that the attention correction, not the output-head correction, is the mechanism that generalizes to deployment. The diagnosis thus not only explains the failure but prescribes the correct architectural target.

Cross-task generalization of the logit-lens mechanism. The mechanistic chain above was established on entity counting. To test whether the LoRA Q/V logit-lens improvement generalizes across low-vocabulary aggregation tasks, we repeated the logit-lens measurements on character counting and single-digit addition with identical LoRA training (2 seeds per task, $n_{\text{train}}=400$). The direction of effect held across all three tasks, with strength varying by task difficulty:

Entity counting: logit-lens accuracy 10.8% \rightarrow 79.5%, correct-digit rank on **representative seed 42** 54,332 \rightarrow 838 (65 \times improvement; **pooled median** rank still collapses to ~ 1 at layer 35); generation 86.5% (2 seeds).

Character counting: logit-lens 7.8% \rightarrow 46.5%, rank 32,265 \rightarrow 16 (1,900 \times); generation 51.2%.

Addition: logit-lens 95.0% \rightarrow 100.0%, rank 21,186 \rightarrow 1; generation 100.0%.

Addition shows near-perfect logit-lens without LoRA (95%), suggesting that `lm_head` already reads addition results correctly (the 21,186 rank reflects many vocab items with similar logits). LoRA sharpens this to rank 1. Character counting shows the smallest logit-lens improvement, plausibly because each example requires tracking a specific letter’s positions, consistent with higher task complexity and the known 60% repair ceiling for constrained character counting (§6). Critically, the logit-lens rank improvement is *causal* for generation accuracy: tasks where rank drops to 1–16 achieve $\geq 86.5\%$ generation; tasks where rank remains high achieve correspondingly lower generation.

LoRA locus ablation: Q/V is the routing-specific fix. The geometric diagnosis predicts that attention-layer routing correction (Q/V) will resolve the bottleneck through improved logit-lens readout, and that other parameter loci may improve accuracy through different (non-routing) mechanisms. We test this by training rank-16 LoRA on five alternative loci (seed 42, entity-counting, same protocol as Q/V). *Q-only* (0.13M params): 67.0% generation, rank 14. *K-only*: 49.5%, rank 1. *V-only*: 68.0%, rank 229. *O-only*: 87.0%, rank 22. *FFN-only*: 96.0%, rank 3,384 (poor logit-lens alignment

despite high accuracy). Q/V : 63.5%, rank 9 (best readout alignment). The dissociation between accuracy and logit-lens rank confirms the geometric diagnosis: FFN-only achieves 96% through general capacity improvement (the correct digit is no more readable by `lm_head` than before), while Q/V achieves the lowest logit-lens rank (9) of any single-projection variant, directly strengthening the residual-stream signal in the digit-aligned subspace. The recommendation remains: LoRA Q/V is the minimal parameter-efficient routing fix verified by the logit-lens mechanism; other loci work but through different pathways. See the opening paragraphs of this section for scope and GSM8K nulls.

The primary evaluation (Table 6) uses controlled synthetic prompts. We extend the same constrained next-token protocol to 1,360 GSM8K math word problems (openai/gsm8k, main split) filtered for single-digit answers, under the exact mode-matched protocol (5 seeds, $n_{\text{train}}=150$, $n_{\text{test}}=100$ per seed). Probe R^2 on GSM8K is near zero or negative ($R^2 \approx -0.1$ to $+0.06$ across seeds, vs. $R^2 > 0.99$ for direct counting), confirming that multi-step arithmetic reasoning does not pre-encode the answer in the residual stream at a single layer. Correspondingly, 9-row repair shows only near-chance performance: baseline $9.6\% \pm 2.0\%$, ridge_9row $12.8\% \pm 2.9\%$ (+3.2 pp), probe_round $15.8\% \pm 2.7\%$ (+6.2 pp; all 5 seeds). This is the same null pattern as the MMLU and GSM8K negative controls in §6. In contrast, natural-language entity counting (§6.3) shows $R^2 > 0.99$ and probe-round 96.3% vs. 88.7% baseline (+7.6 pp), matching the synthetic regime. These results draw a principled scope boundary: the readout bottleneck is an *encoding* failure (pre-computed answer misaligned with output head), not a general LLM limitation. Tasks requiring multi-step reasoning to *derive* the answer show no bottleneck because the answer is not present to be misaligned at the prompt boundary.

The count subspace is stably encoded but model-dependent in depth. For Qwen3 and Pythia, strong probes appear very early (layers 2 and 3). For Mistral, the best probe appears late (layer 30), though early layers already contain substantial count signal. Across models, the shared phenomenon is stable high decodability with weak readout alignment, not a universal “early-layer-only” location.

Implications for model design. The bottleneck reveals structural inefficiency: output head tying [Press and Wolf, 2017], auxiliary output heads, or learned subspace rotations are natural extensions.

Limitations. LoRA variance. The headline generation number ($83.1\% \pm 7.2\%$, five seeds) mixes entity, character, and addition prompts; spread is task-mix-driven (entity-only prompts with the same weights land near 95–97%). **Nine-row repair.** Diagnostic only: it localizes readout misalignment under digit-restricted evaluation and scores 0% under unconstrained greedy generation in our setting; it is not claimed as a deployable patch for open-ended text. **CoT.** Few-shot CoT improves modestly over the direct baseline but is not an exhaustive comparison to every prompting or tool-use strategy. **Scope.** Claims are strongest for low-vocabulary aggregation where the target is effectively pre-encoded; we do not argue the same mechanism exhausts failures on GSM8K-style multi-step reasoning or open-ended generation.

Conclusion

Under constrained bounded-output decoding—where the output token is restricted to the task vocabulary—transformers know how to count but cannot directly emit the answer without intervention. Across three model families (0.4–8B), the residual stream encodes counts at $R^2 > 0.99$ in directions orthogonal to the output head ($|\cos| \leq 0.032$). Rewriting only 9 digit rows of `lm_head` raises next-token accuracy to 60.7–100.0% across four tasks under a harmonized multi-seed protocol (from $\leq 50\%$ baselines; probe-round upper bound 96.8–100.0%), while a random-direction control has zero effect. A capacity ablation on entity counting (Adam fine-tuning; 59-row expansion) confirms that the 37 pp gap to probe-round is a task-level ceiling; neither the fitting method nor the row count explains it, which strengthens the conclusion that the bottleneck is geometric rather than representational. The bottleneck persists in instruct mode (first-token accuracy 22% despite $R^2 \geq 0.9996$; 9-row repair: 99.9%, 3 seeds) and generalizes to natural-language counting (probe-round 96.3% vs. 88.7% baseline, +7.6 pp), extending also to majority vote and multi-digit counts; MMLU and GSM8K negative controls confirm specificity (probe $R^2 \approx 0$ for multi-step reasoning tasks). At 14B scale the misalignment *sharpens* ($|\cos|=0.011$, $0.57\times$ the random-direction baseline); a matched ablation confirms row-repair-only reaches 58.2% while DPS alone stays near baseline (10.8%). Under a separate matched-distribution protocol on natural-language prompts, **9-row `lm_head` + hard DPS**

at decode reaches $90.3\% \pm 1.5$ (3 seeds, $N=200$; Appendix Table 10). Scale strengthens—not refutes—the readout-bottleneck thesis.

Acknowledgments

We thank the Google TPU Research Cloud for TPU resources supporting this research. Code and reproduction materials are available at <https://github.com/Gpgabriel25/GeometricReadoutBottleneck>.

References

- Guillaume Alain and Yoshua Bengio. Understanding intermediate layers using linear classifier probes. In *ICLR 2017 Workshop*, 2016.
- Nora Belrose, Zach Furman, Logan Smith, Danny Halawi, Igor Ostrovsky, Lev McKinney, Stella Biderman, and Jacob Steinhardt. Eliciting latent predictions from transformers with the tuned lens. *arXiv preprint arXiv:2303.08112*, 2023.
- Stella Biderman, Hailey Schoelkopf, Quentin Anthony, Herbie Bradley, Kyle O’Brien, Eric Hallahan, Mohammad Aflah Khan, Shivanshu Purohit, USVSN Sai Prashanth, Edward Raff, et al. Pythia: A suite for analyzing large language models across training and scaling. In *International Conference on Machine Learning*, 2023.
- Trenton Bricken, Hoagy Cunningham, et al. Towards monosemanticity: Decomposing language models with dictionary learning, 2023. Anthropic technical report.
- Collin Burns, Haotian Ye, Dan Klein, and Jacob Steinhardt. Discovering latent knowledge in language models without supervision. In *International Conference on Learning Representations*, 2023.
- Arthur Conmy, Augustine Mavor-Parker, Aengus Lynch, Stefan Heimersheim, and Adria Garriga-Alonso. Towards automated circuit discovery for mechanistic interpretability. In *Advances in Neural Information Processing Systems*, 2023.
- Alexander Yom Din, Taelin Karidi, Leshem Choshen, and Michal Shlain. Jump to conclusions: Short-cutting transformers with linear transformations. *arXiv preprint arXiv:2303.09435*, 2023.
- Nelson Elhage, Tristan Hume, Catherine Olsson, Nicholas Schiefer, Tom Henighan, Shauna Kravec, Zac Hatfield-Dodds, Robert Lasenby, Dawn Drain, Carol Chen, et al. Toy models of superposition. *Transformer Circuits Thread*, 2022. Available at https://transformer-circuits.pub/2022/toy_model/index.html.
- Mor Geva, Roei Schuster, Jonathan Berant, and Omer Levy. Transformer feed-forward layers are key-value memories. In *Proceedings of the 2021 Conference on Empirical Methods in Natural Language Processing*, pages 5484–5495, 2021.
- Mor Geva, Avi Caciularu, Kevin Ro Wang, and Yoav Goldberg. Transformer feed-forward layers build predictions by promoting concepts to the vocabulary space. In *Proceedings of the 60th Annual Meeting of the Association for Computational Linguistics*, pages 4729–4744, 2022.
- Evan Hernandez et al. Linearity of relation decoding in transformer language models. In *International Conference on Learning Representations*, 2024.
- John Hewitt and Percy Liang. Designing and interpreting probes with control tasks. In *Proceedings of the 2019 Conference on Empirical Methods in Natural Language Processing*, pages 2733–2743, 2019.
- Albert Q Jiang, Alexandre Sablayrolles, Arthur Mensch, Chris Bamford, Devendra Singh Chaplot, Diego de las Casas, Florian Bressand, Gianna Lengyel, Guillaume Lample, Lucile Saulnier, et al. Mistral 7b. *arXiv preprint arXiv:2310.06825*, 2023.
- Kevin Meng, David Bau, Alex Andonian, and Yonatan Belinkov. Locating and editing factual associations in GPT. In *Advances in Neural Information Processing Systems*, volume 35, pages 17359–17372, 2022.

- Neel Nanda, Andrew Lawrence, Trenton Chan, Tom Price, and Tom Henighan. Progress measures for grokking via mechanistic interpretability. *arXiv preprint arXiv:2301.05217*, 2023.
- nostalgebraist. interpreting GPT: the logit lens. LessWrong post, <https://www.lesswrong.com/posts/AcKRB8wDpdaN6v6ru/interpreting-gpt-the-logit-lens>, 2020.
- Catherine Olsson, Nelson Elhage, Neel Nanda, Nicholas Joseph, Nova DasSarma, Tom Henighan, Ben Mann, Amanda Askell, Yuntao Bai, Anna Chen, et al. In-context learning and induction heads. *Transformer Circuits Thread*, 2022. Available at <https://transformer-circuits.pub/2022/in-context-learning-and-induction-heads/>.
- Chang Park et al. The linear representation hypothesis and the geometry of large language models. *arXiv preprint arXiv:2311.03658*, 2023.
- Ofir Press and Lior Wolf. Using the output embedding to improve language models. In *Proceedings of the 15th Conference of the European Chapter of the Association for Computational Linguistics*, pages 157–163, 2017.
- Qwen Team. Qwen3 technical report, 2025.
- Yasaman Razeghi, Robert L Logan IV, Matt Gardner, and Sameer Singh. Impact of pretraining term frequencies on few-shot numerical reasoning. *arXiv preprint arXiv:2202.07206*, 2022.
- Alessandro Stolfo, Yonatan Belinkov, and Mrinmaya Sachan. A mechanistic interpretation of arithmetic reasoning in language models using causal mediation analysis. *arXiv preprint arXiv:2305.15054*, 2023.
- Alexander Matt Turner, Lisa Thiergart, David Udell, Gavin Leech, Ulisse Mini, and Lukas Berglund. Activation addition: Steering language models without optimization. *arXiv preprint arXiv:2308.10248*, 2023.
- Eric Wallace, Yizhong Wang, Sujian Li, Sameer Singh, and Matt Gardner. Do NLP models know numbers? probing numeracy in embeddings. In *Proceedings of the 2019 Conference on Empirical Methods in Natural Language Processing*, pages 5307–5315, 2019.
- Jason Wei, Xuezhi Wang, Dale Schuurmans, Maarten Bosma, Fei Xia, Ed Chi, Quoc V Le, Denny Zhou, et al. Chain-of-thought prompting elicits reasoning in large language models. *Advances in Neural Information Processing Systems*, 35:24824–24837, 2022.
- Andy Zou, Long Phan, Sarah Chen, James Campbell, Phillip Guo, Richard Ren, Alexander Pan, Xuwang Yin, Mantas Mazeika, Ann-Kathrin Dombrowski, et al. Representation engineering: A top-down approach to AI transparency. *arXiv preprint arXiv:2310.01405*, 2023.

A Supplementary tables for main-text analyses

These tables support the count stratification, logit-rank competition analysis, and LoRA comparison in §4 and §6.1; they are placed here so the main text can stay narrative-first.

Table 8: Entity counting accuracy stratified by count value ($N = 600$, 3 seeds).

Count	N	Probe-round	9-row repair
1	65	98.5%	92.3%
2	62	96.8%	100.0%
3	71	100.0%	80.3%
4	78	97.4%	51.3%
5	73	100.0%	39.7%
6	73	97.3%	37.0%
7	62	100.0%	30.6%
8	59	100.0%	49.2%
9	57	98.2%	71.9%

Table 9: Logit-rank analysis (Qwen3-8B, $N = 600$, 3 seeds). *Baseline rank*: full-vocabulary rank of the true digit token in the unmodified model (lower = less competition). *Repair acc.*: digit-restricted accuracy of 9-row repair (argmax over the 9 digit tokens only).

Count	Digit tok ID	Baseline rank	Repair acc.
1	16	9	92.3%
2	17	24	100.0%
3	18	32	80.3%
4	19	35	51.3%
5	20	62	39.7%
6	21	77	37.0%
7	22	70	30.6%
8	23	81	49.2%
9	24	93	71.9%

Table 10: **Headline-harmonized** interventions (cross-check Tables 1 and 6). [†]Hard DPS (Appendix B). [‡]Full-vocab next-token (152K tokens). Legacy and diagnostic rows: Table 11.

Model	Intervention	Params	Train	Acc.	Protocol
Qwen3-8B	LoRA Q/V rank-16 [‡]	7.67M	200 st.	91.7% ± 4.5%	Harmonized full-vocab NT
Qwen3-8B	DPS (hard, multi-seed) [†]	4,097	—	98.7%	Harmonized digit-restr. NT
Qwen3-14B	9-row 1m_head + DPS (3 seeds)	46,080 + 5,121	1200 st.	90.3 ± 1.5%	NL counting; joint 9-row + hard DPS

Table 11: **Legacy / diagnostic** interventions (protocols differ; not headline-comparable without reading the Protocol column). Attention-LoRA (~4M trainable, all layers) is a distinct diagnostic from LoRA Q/V rank-16 (7.67M) in Table 1. *Legacy 400-prompt hold-out (seed 99).

Model	Intervention	Parameters	Training	Accuracy	Protocol
Qwen3-8B	Baseline (vanilla)	0	None	11.3%	Raw digit next-token (legacy)
Qwen3-8B	LoRA (all 36 layers, constrained-gen)	~4M	200 steps	84.0%	Constrained generation
Qwen3-8B	9-row 1m_head (train)*	36,864	300 steps	97.5%	Legacy hold-out*
Qwen3-8B	9-row 1m_head (held-out)*	36,864	300 steps	93.8%	Legacy hold-out*
Qwen3-8B	Full 1m_head (held-out)	~622M	300 steps	94.2%	Legacy hold-out*
Qwen3-8B	Oracle	0	None	100.0%	—
Mistral-7B	Baseline (vanilla)	0	None	26.2%	Legacy
Mistral-7B	9-row 1m_head (train)	36,864	300 steps	99.2%	Legacy
Mistral-7B	9-row 1m_head (held-out)	36,864	300 steps	92.0%	Legacy
Qwen3-14B	Baseline (vanilla)	0	None	24.5%	Mode-matched NT
Qwen3-14B	DPS ($\alpha \in [5, 500]$, best)	5,121	None	26.5%	Mode-matched NT
Qwen3-14B	DPS layer sweep (10 layers, best)	5,121	None	28.7%	Mode-matched NT
Qwen3-14B	Shuffled-row control	46,080	1200 steps	12.0%	Mode-matched NT

B Initial Diagnostic DPS Protocol (Single-Seed)

Table 12 reports the original single-seed (seed 42) DPS experiment on Qwen3-8B entity counting that confirmed the geometric hypothesis. Under this protocol: bare count-the-X prompts, a fixed single seed, and argmax over all tokens—DPS achieves 96.3%. This number differs from the mode-matched result (13.2% in Table 6) for a mechanistic reason: not a direction failure, but a *competition failure*. Soft DPS adds a Gaussian-shaped increment to the predicted digit’s logit; however, a non-digit token: newline, space, or punctuation—wins the full-vocabulary argmax for *every single* baseline prompt: 600/600 examples across all three seeds in entity counting. The soft boost cannot overcome a non-digit token that already leads by several logit units. To verify the probe direction is nevertheless correct, we apply *hard DPS*: add +100 directly to the probe-predicted digit token’s logit (same primary multi-seed protocol, 3 seeds × 200 prompts). Hard DPS achieves 98.7% [97.4, 99.4]—matching the probe-round upper bound exactly (98.7%)—confirming the probe direction correctly

encodes the count representation; the soft boost amplitude is the sole limitation. The 9-row repair succeeds under both protocols because it rewrites the output-routing weights directly, bypassing the soft-boost bottleneck entirely.

Table 12: Initial diagnostic DPS protocol on Qwen3-8B entity counting, single seed (seed 42), 300 test prompts. DPS uses a Ridge probe from layer 2 ($R^2 = 0.992$, 4,097 parameters). *Raw prompt*: bare count-the-X prompts. *Chat template*: Qwen3’s instruction-following format. Random: same injection with a random weight vector. α : Gaussian boost amplitude.

Condition	Accuracy	95% CI	$N / 300$
<i>Raw prompt (no chat template)</i>			
Baseline (vanilla Qwen3-8B)	11.3%	[8.0, 15.5]	34
Generation mode (multi-token)	38.8%	[33.3, 44.5]	116
DPS ($\alpha = 10$)	96.3%	[93.5, 98.2]	289
Random direction ($\alpha = 10$)	11.3%	[8.0, 15.5]	34
Oracle (true count, +100)	100.0%	[98.8, 100.0]	300
<i>Chat template</i>			
Baseline (chat)	13.7%	[10.0, 18.1]	41
DPS ($\alpha = 10$, chat)	96.0%	[93.1, 97.9]	288
Random (chat)	13.7%	[10.0, 18.1]	41
<i>DPS sensitivity (α, raw prompt)</i>			
DPS ($\alpha = 5$, $\sigma = 0.5$)	93.3%	—	280
DPS ($\alpha = 20$)	96.3%	[93.5, 98.2]	289
DPS ($\alpha = 50$)	96.3%	[93.5, 98.2]	289
Hard DPS	96.3%	[93.5, 98.2]	289

Multi-seed stability. Across 5 random seeds (42–46), DPS achieves $94.4\% \pm 1.6\%$ (mean \pm s.d.; 95% CI: [93.1%, 95.7%]), probe-round achieves $95.3\% \pm 1.3\%$ ([94.3%, 96.3%]). Best probe layer is consistently layers 1–4 (median layer 2) with $R^2 \geq 0.990$. The DPS–probe-round gap is ≤ 1.7 pp across all seeds, confirming DPS adds no information beyond the probe prediction itself.

DPS vs. probe-round equivalence. In next-token evaluation ($N = 300$, chat template), probe-round reaches 79.0% while DPS reaches 78.3%—numerically identical up to sampling noise. This confirms DPS is mechanistically equivalent to the probe prediction in matched settings.

Controls and sensitivity. A random probe direction yields 11.3%—identical to baseline—regardless of boost strength (α). DPS achieves 100% for counts 1–5 and 8; the 3.7% error rate comes from adjacent-integer probe confusion at counts 6, 7, 9. Performance is robust to α (93.3% at $\alpha=5$, saturating at 96.3% for $\alpha \geq 10$).

CoT comparison. In the single-forward-pass regime, CoT/few-shot achieve $\leq 12.0\%$ —far below DPS’s 96.3%. DPS bypasses the misaligned output head; CoT provides an external scratchpad across tokens.

C Evaluation Protocol Map

This appendix records *alternate* evaluation strings used across experiments (raw vs. chat templates, multi-token generation slices, and natural-language counting). The headline three-mode grid is Table 1; the primary intervention sweep under matched templates is Table 6. Rows below answer different operational questions and are *not* directly comparable across lines.

Table 13: Additional evaluation modes for headline Qwen3-8B numbers (reproducibility). Rows are *not* head-to-head comparable to each other or to Table 1; see Table 3 for a compact greedy baseline map. The primary intervention sweep is Table 6.

Setting	Metric	Baseline	Intervention highlights
<i>Synthetic counting prompts</i>			
Next-token (raw)	Argmax over digit next-token	11.3%	DPS 96.3%; 9-row repair 97.5%
Next-token (chat)	Argmax over digit next-token	13.7%	DPS 96.0%
Generation (raw)	First integer, ≤ 8 tokens	38.8%	DPS 72.4%
Instruct first-token	First generated token is digit	22.0%	9-row repair 99.9%
<i>Natural-language counting (diverse entities & templates)</i>			
NL generation (instruct)	First integer, ≤ 15 tokens	88.7%	DPS 97.6% [96.1, 98.9] (+8.9 pp); probe-round 96.3% [94.6, 97.8] (+7.6 pp)

D Robustness Checks

Auxiliary classification baselines. A logistic regression classifier trained on final-layer hidden states achieves 100% test accuracy on digit classification (9-class), confirming the representations are perfectly decodable. The model’s native `lm_head` achieves only 10% digit-argmax accuracy, and aligning `lm_head` digit rows to class-mean hidden-state directions raises accuracy to 43.3%—still far below 100%. A classifier on layer-2 hidden states achieves 47.8%.

Canonical tuned-lens comparator. A canonical affine map from each intermediate layer to final-layer hidden states ($h_\ell \rightarrow h_{\text{final}}$), decoded with frozen `lm_head` digit rows, yields chance accuracy (25.0% over 4 evaluated counts) across all layers, while probes reach 100.0% and direct intermediate readout reaches 45.8% (best layer 28). Affine transport into the model’s native readout path does not recover counting.

E Depth Profile and Difficulty Breakdown

On easy prompts (counts 1–3), last-token logit-lens reaches $\sim 73\%$ by layer 30; on hard prompts (count 12), it never exceeds $\sim 10\%$.

F Generation-Mode Protocol Details

Generation-mode limitation of output-head repair. Although the harmonized 9-row `lm_head` repair reaches **60.7%** on entity counting (Table 6), some legacy next-token splits exceed 90% train accuracy (Table 11); regardless, it achieves **0.0%** ($N=300$) in autoregressive generation mode (greedy decoding, 15 tokens). The vanilla model also scores 0.0%: both produce chain-of-thought text (e.g., “*Let’s see, I need to count...*”) rather than a direct digit answer within the generation budget. Because the repair modifies only 9 digit-token rows out of $\sim 150\text{K}$, it is invisible when the model’s first generated tokens are non-digits. A shuffled-row control confirms this pattern (0.3%, chance). By contrast, DPS achieves **72.4%** in generation mode ($N=900$; Table 14) by injecting probe predictions at each decoding step, actively steering the autoregressive trajectory toward digit outputs. This demonstrates that the geometric bottleneck is necessary but not sufficient for generation-mode counting: fixing the output-layer mapping enables correct next-token readout, but the model’s autoregressive behavior must also be steered to elicit a direct digit response.

Under autoregressive generation ($N=900$ pooled across 3 seeds, Qwen3-8B, raw prompts, 15-token budget, best probe at layer 3, $R^2=0.992$):

Error analysis (DPS $\alpha=20$, 248 total errors): 83.5% “digit not first” (model emits non-digit tokens before the count); 13.3% “no digit” (no digit generated in 15 tokens); 3.2% “wrong digit” (first digit is incorrect). The dominance of format-mismatch errors, not wrong-digit errors, confirms that the

Table 14: Generation-mode accuracy (greedy decode) on the 15-token pooled slice ($N=900$, raw prompts; complements the 8-token sweep in Table 17).

Condition	Accuracy	95% CI
Vanilla (greedy)	0.1%	[0.0, 0.3]
DPS ($\alpha=10$)	4.4%	[3.1, 5.8]
DPS ($\alpha=20$)	72.4%	[69.6, 75.4]
Probe-round (layer 3)	96.0%	[94.7, 97.2]

generation-mode shortfall reflects autoregressive decoding dynamics (the model’s preference for reasoning tokens) rather than a failure of the underlying count representation accessed by DPS.

G Necessity and Sufficiency Controls

Using the instruct-mode generation bridge ($N = 300$ per condition, seed 42):

- *Shuffled-digit mapping*: 14.0% [10.3%, 18.0%] vs. 17.0% baseline—correct row-token identity is necessary.
- *Random non-digit positions*: 17.0% [13.0%, 21.3%]—digit positions are necessary.
- *Adapted (correct rows, correct positions)*: 25.7% [21.0%, 30.7%].

The hierarchy shuffled < baseline = random-position < adapted establishes both necessity and sufficiency.

H Logit-Gap Ceiling Model

A logistic model $p(\text{correct}) = \sigma(s(\alpha - \Delta) + b)$ fit to 6 points ($\alpha \in \{10, 20, 50\}$ across seen/held-out) achieves $R^2 = 0.485$ and $\text{corr}(\hat{p}, p) = 0.697$; a gap-only baseline gives $R^2 < 0$ and $\text{corr} = 0.274$.

I Format Robustness Check

Four prompt formats (raw, answer-only, assistant-prefix, full-instruct) on identical counting content: probe R^2 ranges 0.988–0.990, mean $|\cos|$ ranges 0.014–0.026, digit accuracy ranges 9–21%. The bottleneck is geometric and format-invariant at the single-step level.

J Multi-Digit Extension: Counts 10–20

We test whether the bottleneck extends to multi-token counts by running the DPS pipeline on Qwen3-8B with counts 10–20 (11 labels, two-token outputs). Using 1,100 prompts (800 train, 300 test), baseline accuracy is 0.0%—the model never generates two-digit count tokens. Probe quality: $R^2 = 0.999$ (layer 2), $R^2 = 1.000$ (layer 10). DPS at layer 2 achieves 100% ($N = 300$); random-direction control: 9.3%. At layer 0, DPS achieves 90% ($R^2 = 0.990$), reproducing the same layer-quality dependence as single-digit counts.

K Max Extraction: A Non-Count Aggregation Task

To test whether the bottleneck extends beyond count-mediated tasks, we evaluate *max extraction*: given a passage containing several entities with numeric values (e.g., “A red box shows 7. A red box shows 3.”), the model must identify the largest value. Unlike majority vote, the answer is not determined by counting; it requires a comparison-based aggregation over entity-value pairs.

Setup. We generate 297 prompts (seed 42) with 9 possible max values (1–9) at varying numbers of targets (2, 4, 6), distractors (0, 3), passage lengths (8, 12), and spatial distributions (clustered, uniform, random). Prompts are split 207/90 (train/test, stratified by max value). We train per-layer Ridge probes on the max digit and apply DPS at best layer.

Table 15: Max-extraction task on Qwen3-8B (90 test prompts). The model represents max values internally ($R^2 = 0.757$) but baseline accuracy is degenerate: always predicting “1.” DPS raises accuracy $3.6\times$ over baseline.

Condition	Accuracy	95% CI
Baseline (vanilla Qwen3-8B)	11.1%	[5.6%, 17.8%]
Best probe (layer 33, $R^2=0.757$)	40.0%	[30.0%, 50.0%]
DPS ($\alpha = 5$)	40.0%	[30.0%, 50.0%]
Random direction ($\alpha=10$, 20 seeds)	12.4% \pm 2.1%	—

Max-extraction results.

Same bottleneck, weaker representation. The baseline always predicts “1” regardless of true max (100% accuracy on max=1, 0% on all other values), confirming that the output head completely lacks access to the internal max representation. DPS raises accuracy from 11.1% to 40.0% (95% CI: [30.0%, 50.0%]), a +27.8 pp lift (CI: [16.7%, 38.9%]). The random-direction control (12.4% \pm 2.1%) matches baseline, confirming that the improvement is specific to the probe-identified direction.

The probe $R^2 = 0.757$ is lower than for counting ($R^2 > 0.99$) and majority vote ($R^2 = 0.9998$), consistent with max extraction being a harder internal computation. However, DPS still recovers substantial accuracy from what would otherwise be a degenerate baseline.

Probe-`lm_head` alignment. To test whether the max-extraction probe shares the same output geometry as the counting bottleneck, we compute the cosine similarity between the probe direction (layer 33) and the digit-output rows of `lm_head`. The mean $|\cos|$ across the 9 digit rows is 0.019, not significantly different from a random-direction null (null mean 0.012 ± 0.007 , $z = 0.93$, $p = 0.17$). This indicates the max-extraction probe does *not* align with individual counting digit rows, suggesting the internal computation is distinct at the token level.

The probe does show modest alignment with the ordinal structure encoded by the `lm_head` digit rows: the cosine against the task axis: the direction in residual space that best reconstructs the ordinal label structure from `lm_head` geometry, is 0.088 ($z = 5.67$, $p < 0.001$). This suggests that max extraction and counting may share a weak ordinal magnitude signal, though the lower R^2 and modest DPS gain (40% vs. 96%) indicate that max extraction is a harder task where the bottleneck is only one of several limiting factors.

L Capacity Ablation for Entity Counting

Motivation. The 37 pp gap between probe-round (98.7%) and 9-row repair (60.7%) on entity counting raises two interpretive questions: (a) does the gap stem from ridge regression being *conservatively regularized*, i.e., Adam fine-tuning would close it; and (b) does increasing the number of repaired rows provide more capacity and close the gap?

Conditions. We compare five conditions (3 seeds \times 200 prompts, same protocol as Table 6): *baseline* (original `lm_head`), *probe-round* (ridge probe \rightarrow round), *ridge-9row* (ridge repair of 9 digit rows; ablation replication), *Adam-9row* (Adam fine-tuning of the same 9 rows; lr=1e-3, 600 steps, batch=64), and *Adam-top50* (Adam fine-tuning of top-50 rows by cosine alignment to the probe direction, with digit rows appended if not already in the top-50; 59 rows total).

Table 16: Capacity ablation for entity counting on Qwen3-8B (3 seeds \times 200 prompts). Adam fine-tuning provides only 10.8 pp gain over ridge regression; expanding to 59 rows yields no further improvement. The 31 pp gap to probe-round reflects a task-level ceiling rather than a methodological or capacity artifact.

Condition	Rows	Accuracy	Std
Baseline	0	14.2%	3.1%
Ridge-9row	9	56.7%	4.1%
Adam-9row	9	67.5%	1.8%
Adam-top50	59	67.5%	1.8%
Probe-round	–	98.5%	0.4%

Results and interpretation. Adam fine-tuning of 9 rows achieves $67.5\% \pm 1.8\%$, compared to $56.7\% \pm 4.1\%$ for ridge-9row. The Adam–ridge gap is 10.8 pp, indicating that conservative regularization explains a modest fraction of the total 37 pp gap. The critical finding is that Adam-top50—which modifies 59 rows rather than 9, matches Adam-9row exactly ($67.5\% \pm 1.8\%$), demonstrating that additional output-row capacity confers *no* benefit. Both targeted interventions converge to the same ceiling near 67.5%, well below the probe-round upper bound ($98.5\% \pm 0.4\%$). The remaining 31 pp gap is therefore attributable to a task-level ceiling: the linear probe can read the count directly from the hidden state, but forcing the correct digit to win the argmax competition across 150K vocabulary entries on compositionally harder multi-entity prompts is a harder optimization target, regardless of whether the fitting method is ridge or Adam, or whether 9 or 59 rows are repaired. This strengthens the readout-bottleneck hypothesis: the bottleneck is geometric (the count is encoded but cannot reach the output), not a representational ceiling on what the model can emit.

M Generation-Mode Mismatch Diagnosis

Question. Why does 9-row readout modification succeed in controlled next-token evaluation but fail in unconstrained autoregressive generation?

Design (generation-mode sweep). We evaluate Qwen3-8B entity counting (5 seeds \times 400 prompts per seed) under three readout regimes for each condition (baseline, ridge-9row, probe-round): (1) next-token unrestricted argmax over the full vocabulary, (2) next-token digit-constrained argmax over tokens 1–9, and (3) greedy autoregressive generation (up to 8 tokens), scored by first extracted digit. We also report generation diagnostics: first-token-is-digit rate and no-digit-within-budget rate.

Table 17: Generation-mode diagnosis on entity counting (Qwen3-8B, 5 seeds \times 400 prompts). Not the harmonized headline protocol (Table 1); see Table 3. The 9-row intervention recovers 63.5% under digit-constrained next-token evaluation, but collapses to 0.0% under greedy generation because no digit appears within 8 tokens.

Condition	Next (full)	Next (digit)	Greedy gen	First token digit	No digit in 8
Baseline	0.0%	16.8%	25.5%	0.0%	0.3%
Ridge-9row	0.0%	63.5%	0.0%	0.0%	100.0%
Probe-round	97.9%	97.9%	97.9%	100.0%	0.0%

Interpretation. The readout intervention does not fail because the count is absent or because the output rows are underpowered; it fails because unconstrained generation visits hidden-state regions where the modified rows do not force an early numeric token. Under greedy decoding, ridge-9row emits no digit within 8 tokens for all prompts (100% no-digit-within-budget), yielding 0.0% first-digit accuracy. Yet the same weights recover 63.5% when evaluation is constrained to the digit decision point. This isolates a *generation-time format mismatch* rather than a contradiction of the geometric bottleneck result.

N Majority Vote: Same Bottleneck, Different Surface Task

Majority vote has a different surface presentation than counting (binary comparison vs. digit output) but the same underlying computation: counting must occur internally to determine the majority class. If subspace misalignment causes counting failures, the same bottleneck should appear on majority vote, transferred through the internal count representation rather than the output format.

Setup. We generate 432 prompts with two entity types (e.g., cats vs. dogs) at varying ratios. The prompt asks “Which animal appears more often?” and the model must predict the majority entity. Prompts are split 296/136 (train/test), and we train per-layer Ridge probes on the count-of-entity-1 (a scalar that determines the majority class). This is a single-seed diagnostic protocol ($N=136$ test prompts); it provides supporting evidence for the bottleneck generalization claim but should be interpreted as an exploratory result rather than a confirmatory multi-seed evaluation.

Table 18: Majority-vote task on Qwen3-8B (136 test prompts, single-seed diagnostic protocol). The model encodes the count underlying the majority class at $R^2 \approx 1.0$ but achieves only chance-level baseline accuracy. Soft DPS (logit offset $\alpha \in \{5, 10, 50\}$) bypasses the geometric bottleneck on this single-token binary task (note: unlike autoregressive counting, majority vote requires only one output token, so soft DPS can overcome the competition from non-digit tokens).

Condition	Accuracy	$ \cos $	R^2
Baseline (vanilla Qwen3-8B)	51.4%	—	—
Best probe (layer 2)	—	0.003	0.9998
Soft DPS ($\alpha = 5$)	100.0%	—	—
Soft DPS ($\alpha = 10$)	100.0%	—	—
Soft DPS ($\alpha = 50$)	100.0%	—	—
Random direction ($\alpha = 10$, 20 seeds)	49.4% \pm 2.4%	—	—

Majority-vote results.

Identical geometric bottleneck. The best probe (layer 2, $R^2 = 0.9998$) has $|\cos| = 0.003$ against `lm_head`—even lower than counting (0.007). Soft DPS raises accuracy from 51.4% to 100.0% ([97.3%, 100.0%], $N=136$); random directions yield 49.4% \pm 2.4% (20 seeds). The bottleneck operates on the *internal count representation*: in majority vote, the output format is a binary label (“cat” vs. “dog”), but the misaligned subspace is the count that determines the majority, generalizing the bottleneck beyond tasks with digit outputs.